Relaxed but highly compact diansa metallacyclophanes.

Pau Farràs,[a] Francesc Teixidor,[a] Isabel Rojo,[a] Raikko Kivekäs,[b] Reijo Sillanpää,[c] Patricia González-Cardoso[a,#] and Clara Viñas,[a,*]

[a] Institut de Ciència de Materials de Barcelona (ICMAB-CSIC), Campus de la U.A.B., E-08193 Bellaterra, Spain. Telefax: Int. Code + 34 93 5805729. E-mail: clara@icmab.es.

[b] Department of Chemistry, P.O. Box 55, University of Helsinki, FIN-00014, Finland.

[c] Department of Chemistry, University of Jyväskylä, FIN-40351, Finland.

P.González-Cardoso is enrolled in the UAB PhD program.

Key Words: metallacarboranes, metallocenophanes, monoansa, diansa, phosphanes, electron-transfer.

Abstract

A series of monoansa [μ-1,1'-PR-3,3'-Co(1,2-$C_2B_9H_{10})_2]^-$ and diansa [8,8'-μ-(1'',2''-benzene)-μ-1,1'-PR-3,3'-Co(1,2-$C_2B_9H_9)_2]^-$ (R= Ph, ^{t}Bu) cobaltabisdicarbollidephanes has been synthesized and characterized by NMR, MALDI-TOF-MS, UV/visible spectroscopy, cyclic voltammetry and DFT calculations. Single crystal X-ray diffraction revealed a highly relaxed structure characterized by the title angle α of 3.8º ([**7**]$^-$), this being the smallest angle α for a metallacyclophane. In such compounds, the metal-to-phosphorus distance is less than the sum of their vdW radii. The availability of a phosphorus lone pair causes an electron delocalization through the metal, as shown by the abnormal ^{31}P NMR chemical shift. Remarkably, the combination of a phosphine donor and a phenyl acceptor moieties causes a synergistic effect that is observed through the different techniques used in this study. The importance of having an available lone pair is demonstrated by the oxidation of phosphorus with hydrogen peroxide, sulfur and elemental black selenium to produce the corresponding P^V compounds. When the electron lone pair is used to form the bond with the corresponding chalcogen atom, the communication between the donor and acceptor moieties on the diansa metallacyclophane is shut down.

Introduction

The first examples of sandwich metallacarboranes were prepared 46 years ago by Hawthorne et *al*. using the dicarbollide ion, $[C_2B_9H_{11}]^{2-}$, as ligand to form *closo* $[M(C_2B_9H_{11})_2]^-$ (M= Co, Fe) icosahedral clusters.[1] The $[C_2B_9H_{11}]^{2-}$ ligand has been compared to $[C_5H_5]^-$, as both behave as formal 6-electron donors[2] to metal atoms via η^5-face bonding. On the other hand, metallocenes have emerged as the most important organometallic compounds to be systematically developed and studied due to their interesting structures, bonding, electrochemical and electronic properties that facilitate a plethora of applications.[3] The first strained ferrocenophane with a C_2Me_4 bridge, monoansa C_2Me_4[2]ferrocenophane, was reported in 1960[4] while, a more strained one with a single Si atom bridge was synthesized in 1975.[5] Later other related single atom bridging compounds with main group elements and transition group metals (bridging atom X= B, Ge, P, As, S, Se, Al, Ga, Sn, Ni, Mn, Ti, Zr, Hf), monoansa X[1]ferrocenophanes have been reported.[6] The single atom ansa causes high strain to the original structure of ferrocene, *fc*, therefore if a second ansa was targeted, this either was adjacent or a multiple atom ansa was required to produce a confronted diansa ferrocenophane. See Chart 1 to visualize the indicated two types of diansa ferrocenophanes, the adjacent and the confronted. We have coined the confronting diansa term to indicate a metallocene with a maximum separation between the two entities, so that one faces the other. Therefore, due to the strain originated by a single atom bridge in a monoansa X[1]ferrocenophane, no example has been published of a fully compact confronted diansa ferrocenophane. The most compact to date confronted ferrocenophane is Me_4C_2*fc*S_3 that can also be written as Me_4C_2[2]S_3[3]ferrocenephane[7] to indicate the length of the two different ansas.

Cobaltabisdicarbollide, [3,3'-Co(1,2-$C_2B_9H_{11})_2]^-$, [**1**]$^-$, is analogous to cobaltocenium ion, $[Co(C_5H_5)_2]^+$, and like the latter it demonstrates a simple reversible $Co^{3+/2+}$ couple in electrolyte solutions of organic solvents with a significant cathodic shift of the $Co^{3+/2+}$ reduction potential (-1.80 V (cobaltabisdicarbollide)[8] *vs*. -1.33 V (cobaltocene),[9] both taking ferrocene as a reference). While the derivative chemistry of metallocenes has been widely studied, the one of [**1**]$^-$ remains very much unexplored.[10] The fundamental reason for this is the synthetic strategy leading to their derivatives. Two basic substitutions may occur on [3,3'-Co(1,2-$C_2B_9H_{11})_2]^-$, either on carbon or on boron. With few exceptions[11] substitutions on carbon have been achieved only at an early stage of the synthetic process i.e. on the starting *o*-carborane,[12] but not by direct reaction at the [3,3'-Co(1,2-$C_2B_9H_{11})_2]^-$ cage. Substitution at boron has been accomplished under Friedel-Crafts conditions,[13] Kumada[8,14] and Heck[15] reactions or with strong alkylating agents.[2a,14a,16]

The structurally and coordinately similar $[C_2B_9H_{11}]^{2-}$ and $[C_5H_5]^-$ ligands differ in their charges, which influence on their capacity to stabilize high oxidation states[2a] and the out of plane disposition of the open face substituents.[17]

Our aim in presenting this work has been the synthesis of relaxed monoansa phospha[1]cobaltabisdicarbollidephanes as well as the first example of a relaxed and highly compact diansa metallocenephane: the diansa phospha[1]benzene[2]cobaltabisdicarbollidephanes, in order to establish possible interactions between the P atom bridge and its available lone pair from an ansa and the metal of the metallacyclophane modulated by a confronting second ansa. It was expected that this confronting two ansa system could tune the structural, electronic and electrochemical properties of the complex. Oxidation of the bridging P to prevent the P lone pair availability within the metallocycle, by using hydrogen peroxide, sulfur and

selenium has also been carried on to bring extra information on the P···M interaction. To gain further insight into the nature of the latter P···M interaction, computational studies on non-oxidized and oxidized monoansa and diansa cobaltabisdicarbollidephanes have been performed. Moreover, the first crystal structure of a compact confronting diansa metallocenephane is reported.

Results

1. Synthesis of mono and diansa cobaltabisdicarbollidephane anions.

The targeted anionic bridged phosphine compounds, monoansa ([**3**]$^-$, [**11**]$^-$**)** phospha[1]cobaltabisdicarbollidephanes and diansa ([**7**]$^-$, [**15**]$^-$) phospha[1]benzene[2]cobaltabisdicarbollidephanes, are conveniently prepared by metallation of Cs[3,3'-Co(1,2-$C_2B_9H_{11})_2$], Cs[**1**], or Cs[8,8'-(1",2"-C_6H_4)-3,3'-Co(1,2-$C_2B_9H_{10})_2$], Cs[**2**], with 2 equivalents of *n*-BuLi, followed by simple reaction with the corresponding dichlorophosphine in 1,2-dimethoxyethane (DME) at low temperature, as shown in Scheme 1. Chart 2 displays the numbering of mono and diansa phospha[1]cobaltabisdicarbollidephane anions synthesized in this paper. The $[NMe_4]^+$ salts can be produced by metathesis dissolving Li^+ salts in ethanol and adding an aqueous solution of $[NMe_4]Cl$. Solids corresponding to $[NMe_4]^+$ salts separate well and can be collected by filtration. Column chromatography is needed to purify the compounds by using a dicloromethane/acetonitrile mixture (70/30). Yields are in the range 51-71%.

The monoansa phospha[1]cobaltabisdicarbollidephane and diansa phospha[1]benzene[2]cobaltabisdicarbollidephane anions may exist at least in four structural/spatial isomers: *meso*, mixed and racemic mixture, respectively (Figures 1 and 2). Each of these isomers converts into two when the inversion at P is contemplated.

Therefore two *meso*, two mixed and two racemic mixtures could be generated. The isomers resulting from P inversion need to be accounted for because typical inversion barriers for tertiary phosphines are in the range 28-36 kcal·mol^{-1}.

All monoansa and diansa cobaltabisdicarbollidephane mixtures were characterized by elemental analysis (EA), IR, MALDI-TOF-MS, ^{1}H, ^{13}C{^{1}H}, ^{31}P{^{1}H} and ^{11}B NMR spectroscopies. The combination of these techniques has been very valuable to characterize the structures shown in Chart 2. MALDI-TOF-MS and EA have provided the constitutional purity of the compounds, whereas NMR spectra have provided information about the geometrical isomers present. In this regard, and as an example, Figure 5a shows the experimental and calculated patterns for the molecular ion peak of anion [**3**]$^{-}$. The IR spectra of all compounds present typical υ(B-H) strong bands for *closo* clusters between 2554 and 2577 cm^{-1}.

More information on the isomeric composition could be drawn from the experimental ^{11}B{^{1}H} NMR spectra for anions [**3**]$^{-}$ and [**7**]$^{-}$ that are on display in Figures 3 and 4. There it can be seen a larger number of resonances in the range δ= +8.3 to -22.7 ppm for [**3**]$^{-}$ and [**7**]$^{-}$ with respect to their precursors [**1**]$^{-}$ and [**2**]$^{-}$. This implies that at least two geometrical isomers are present in solution. The two low-field resonances for [**7**]$^{-}$ in Figure 4a do not split in the ^{11}B NMR spectrum and, by comparison with the ^{11}B NMR of [**2**]$^{-}$, have to be attributed to the B(8)/B(8') atoms bonded to the benzene bridging group. The different intensities of the two low field resonances in [**7**]$^{-}$ (Figure 4b) are consistent with the coexistence of two isomers as it is the ^{31}P{^{1}H} NMR spectra of [**3**]$^{-}$, [**7**]$^{-}$, [**11**]$^{-}$ and [**15**]$^{-}$ with two resonances each (see Table 1). The ^{1}H NMR spectrum of [**3**]$^{-}$ displays a group of resonances between δ = 7.64 and 7.48 ppm corresponding to the aromatic hydrogen atoms and two sets of broad singlets, one at δ = 5.70, 5.30 ppm and the second at δ =4.59, 4.41 ppm with a ratio 11:2 corresponding to the C_c-H hydrogen

atoms (C_c = cluster carbon atom). The presence of two sets of resonances was also in agreement with the presence of two isomers. Finally, the $^{13}C\{^1H\}$ NMR spectrum of [**3**]$^-$ also shows the resonances of the two isomers. The fact that all this variety of techniques have given indication of only two isomers, seem to suggest that with high probability only two isomers coexist in solution. An X-ray diffraction study of [NMe_4][**7**] confirmed that one of the synthesized geometrical isomers was indeed the *meso* form.

Crystal structure of [NMe_4][7].

Crystals of [NMe_4][**7**] suitable for an X-ray diffraction study were obtained by slow evaporation of the solvent from a solution of the compound in dichloromethane. The crystals have the formula [NMe_4][**7**]·0.8CH_2Cl_2. In solid state (space group $P2_1/c$) the structure consists of well-separated $[NMe_4]^+$ cations, diansa cobaltabisdicarbollidephane [**7**]$^-$ anions and dichloromethane molecules. The [**7**]$^-$ anions (two rotamers at the same position in a ratio of 4:1) are disordered. If the major rotamer **a** (the atoms labelled with an **a** affix represent the main rotamer) is present then also a dichloromethane molecule is present. Figure 6a shows a drawing of such a situation. Figure 6b shows the situation when rotamer **b** is in the asymmetric unit. In such case dichlomethane is not present as the P1b ··· C1 distance is 2.88 Å. Figure 6c shows the asymmetric unit as a whole. In rotamer **a** (in this part of disordered [**7**]$^-$ anions show reasonable geometrical parameters) the Co3 ··· P1a distance is 2.769(1) Å , which is longer than the covalent radii of Co and P (231 pm) but much shorter than the sum of van der Waals radii's of the atoms (380 pm). The cage bridging distances, C1−P1a and C1'−P1a are 1.863(4) and 1.915(4), respectively. The bridging angle, C1−P1a−C1' is 92.6(2)°, is distorted from ideal tetrahedral angle (109.5) ° due to the bond to the rigid boron cages.

As expected, the metal in [**7**]$^-$ is sandwiched by the pentagonal faces of the two dicarbollide units. The pentagonal faces have a mirror conformation, with the torsion

angle C1-c_t-c_t'-C1' being 0.88º (c_t = the centroid of C1, C2, B7, B8, B4 face; c_t' = the centroid of C1', C2', B7', B8', B4' face). Thus, the dicarbollide moieties have a *meso* disposition as was observed with the silicon monoansa compound [1,1'-$SiMe_2$-3,3'-$Co(1,2\text{-}C_2B_9H_{10})_2]^-$, [**21**]$^-$.[11b]

2. Synthesis of the mono and diansa cobaltabisdicarbollidephane oxidized anions with oxygen, sulphur and selenium.

The reasonable stability of these monoansa phospha[1]cobaltabisdicarbollidephane ([**3**]$^-$, [**11**]$^-$) and diansa phospha[1]benzene[2]cobaltabisdicarbollidephane ([**7**]$^-$, [**15**]$^-$) compounds under air has required the use of hydrogen peroxide in acetone at room temperature or sulphur or selenium in refluxing acetone for 30h to be oxidized to their corresponding monoansa phospha(E)[1]cobaltabisdicarbollidephanes, [**4**]$^-$, [**5**]$^-$, [**6**]$^-$, [**12**]$^-$, [**13**]$^-$ and [**14**]$^-$, and diansa phospha(E)[1]benzene[2]cobaltabisdicarbollidephane, [**8**]$^-$, [**9**]$^-$, [**10**]$^-$, [**16**]$^-$, [**17**]$^-$ and [**18**]$^-$, (E= O, S, Se). After work-up the compounds were obtained in very good yields (86-97%). Monoansa and diansa phospha[1]cobaltabisdicarbollidephane oxidized species were characterized by EA, IR, MALDI-TOF-MS, ^{1}H, ^{13}C{^{1}H}, ^{31}P{^{1}H} and ^{11}B NMR spectroscopies as reported at the experimental section. Strong broad absorptions at 2644-2550 cm^{-1} due to B–H stretches dominated the IR spectra. P=O, P=S and P=Se stretches are found as strong and sharp absorptions at 1300-1205, 676-645 or 701-688 cm^{-1}, respectively. In addition, the IR spectra exhibited strong ν(C-H) stretch absorption at 3050-3019 cm^{-1} confirming the presence of C_c-H bonds.

For each of the oxidized species, the *closo* cluster structure was preserved despite changes in the oxidation state from P^{III} to P^V. Table 1 shows the ^{31}P{^{1}H} NMR chemical shift of the oxidized compounds. Most of the resonances appear at a higher

field than those corresponding to the phosphine precursors. The shielding capacity on the $^{31}P\{^{1}H\}$ chemical shift followed the tendency O>Se>S (Table 1).

$^{31}P\{^{1}H\}$ NMR spectroscopy corroborated the P oxidation state, the presence of the P-Se bond in [**6**]$^{-}$, [**10**]$^{-}$, [**14**]$^{-}$ and [**18**]$^{-}$ and the presence of the two geometrical isomers in the oxidized species. Evidence for the formation of the P-Se bond can be drawn from the $^{31}P\{^{1}H\}$ NMR spectra of the anionic ([Co(C_2B_9)$_2$])SePR species. Upon prolonged recording times, two satellite lines due to the $^{1}J(^{31}P,^{77}Se)$ appeared, indicating the presence of a P-Se bond. According to the literature, the coupling constants $^{1}J(^{31}P,^{77}Se)$ can reach values ranging from 500 to 1130 Hz for P=Se.[18] A large $^{1}J(^{31}P,^{77}Se)$ value indicates a strong electron withdrawing capacity of the substituents attached to the phosphorus atom,[19] an increased *s*- character for the phosphorus lone pair[20] and a more positive P atom.[21] The ^{77}Se satellites, $^{1}J(^{31}P,^{77}Se)$= 833, 848, 679 and 692 Hz, centered at 69.8, 71.0, 98.9 and 97.5 ppm for compounds [**6**]$^{-}$, [**10**]$^{-}$, [**14**]$^{-}$ and [**18**]$^{-}$ confirmed the formation of a P-Se bond. The $^{31}P\{^{1}H\}$ NMR resonances for the monoansa [**6**]$^{-}$, [**10**]$^{-}$ and diansa [**14**]$^{-}$ and [**18**]$^{-}$ ([Co(C_2B_9)$_2$])SePR anionic species appeared at lower field than for Ph_3PSe (δ= 35.8 ppm).[22] As shown in Table 1, the coupling constant value $^{1}J(^{31}P,^{77}Se)$= 730 Hz for Ph_3PSe[23] is smaller than the monoansa [**6**]$^{-}$ and [**10**]$^{-}$ but larger than for the diansa [**14**]$^{-}$ and [**18**]$^{-}$ anionic species. Table 1 indicates that the magnitude of the $^{1}J(^{31}P,^{77}Se)$ coupling constant is slightly influenced by the presence of the second ansa (15 Hz) whereas the organic substituent at the phosphorus atom (Ph or ^{t}Bu) produces a considerable tuning (155 Hz).

As discussed, the $^{31}P\{^{1}H\}$ NMR of the oxidized species has clearly shown the coexistence of two isomers in solution, in agreement with the $^{31}P\{^{1}H\}$ and $^{11}B\{^{1}H\}$ NMR of the non-oxidized precursors. This would imply a complicated $^{11}B\{^{1}H\}$ NMR that would account for the two oxidized isomers in solution. Surprisingly, this is not the

case, the 2:2:1:3:2:2:2:2:2, 2:6:2:2:4:2 or 1:1:4:2:2:4:2 patterns in the range δ = +8.6 / –22.8 ppm for the monoansa metallacyclophanes and δ = +26.7 / –26.6 ppm for the diansa metallacyclophanes even with fewer resonances than for the monoansa validate a *closo* cluster with unexpectedly coincidental overlap. Figures 3 and 4 display the experimental $^{11}B\{^{1}H\}$ NMR spectra for oxidized anions [**4**]$^-$ and [**8**]$^-$.

The ^{1}H NMR spectra for [**4**]$^-$, [**5**]$^-$ and [**6**]$^-$ display two groups of resonances with a ratio of 2:3, one at 7.68-7.59 ppm and the second at 8.16-8.09 ppm., that correspond to the hydrogen atoms on the phenyl group. The broadness of these resonances is also indicative of at least two isomers in solution. Importantly, the MALDI-TOF-MS of anion [**6**]$^-$ displays the molecular ion peak at m/z 509.65 and a fragmentation peak at m/z 429.66 corresponding to the lost of H_2Se (Figure 5b).

These techniques have shown the existence of two isomers, but how are they?.

Crystal structures of [NMe_4][4], [NMe_4][5] and [NMe_4][6].

Single crystals suitable for X-ray diffraction studies were grown by slow evaporation of compounds [NMe_4][**4**] and [NMe_4][**5**] in dichloromethane solutions and by slow evaporation of [NMe_4][**6**] in toluene. Table 2 contains the crystal data of the compounds and Table 3 lists selected bond lengths and angles. All three compounds are formed from $[NMe_4]^+$ cations and the relevant anions. The space group of [NMe_4][**4**] is centrosymmetric (C2/c), but for [NMe_4][**5**] **(**$P2_12_12_1$) and [NMe_4][**6**] **(**$P2_1nb$) it is chiral. Compound [NMe_4][**5**] was refined as a racemic twin. Figures 7, 8 and 9 show the structures of the anions: all have a "racemic" conformation. The Co-P distances in all three anions are very close to each other (from 2.767(1) to 2.778(2) Å). For the Co-P distances the similar discussion is valid as for [NMe_4][**7**]. The P=E bond length (O, S, Se) are 1.476(3), 1.9373(16) and 2.0904(14) Å, respectively. The calculated values using covalent radii by Pyykkö[24] are 1.59, 1.96 and 2.09 Å. The measured values

compare well with the distances obtained from the covalent radii by Pyykkö, except for the P=O bond, which is much shorter. If the P=O bond is calculated as a triple bond the value is 1.47. This value is very close to the measured result and comparable to the calculated ones (1.4976 Å for [**4**]$^-$, 1.4937 Å for [**8**]$^-$ and 1.5005 Å for [**12**]$^-$). Other important geometrical parameters are also presented in Table 4. All structural parameters indicate very similar structures for [**4**]$^-$, [**5**]$^-$ and [**6**]$^-$ ions.

The crystal packing of [NMe_4][**4**] reveals two weak P-O1···H-C (C19 and C22) hydrogen bonds (the O···H distances are 2.419 and 2.521 Å, the O···H-C angles are 152 and 148°, respectively). In addition there are weak B-H···H-C interactions between the CH_3 hydrogens of $[NMe_4]^+$ cations and the B-H vertex of the anions to stabilize the structure. The crystal packing of [NMe_4][**5**] and [NMe_4][**6**] reveal only the weak B-H···H-C interactions.

Discussion

1. Structural Details

Ferrocenophanes are the paradigm of metallocenophanes; therefore a structural comparison of the cobaltacyclophanes described in this paper with the equivalent ferrocenophanes is of relevance. In this regard, we have compared the structures of phospha[1]ferrocenophanes and phospha[1]cobaltabisdicarbollidephanes, along with the oxidation products of monoansa phospha[1]cobaltabisdicarbollidephane, [**4**]$^-$, [**5**]$^-$, [**6**]$^-$) and diansa phospha[1]benzene[2]cobaltabisdicarbollidephane [**7**]$^-$. The most remarkable structural features as a result of the strain induced by the phospha-bridge are the tilt angle α, that is positive or negative depending on the opening or closure of the C_2B_3 planes around the Co(III) ion, ([**7**]$^-$: -3.8(3)°; [**4**]$^-$: -9.3(3)°; [**5**]$^-$: -9.3(2)°; [**6**]$^-$: -9.5(3)°) and the angles β and β' (([**7**]$^-$: 44.0 and 44.4°; [**4**]$^-$: 41.4 and 43.3°; [**5**]$^-$: 41.5 and 42.6°;

[**6**]$^-$: 40.9 and 41.9°) (Table 4 and Figure 10). Comparison of the geometrical parameters of these monoansa phospha[1]cobaltabisdicarbollidephane derivatives, [**4**]$^-$, [**5**]$^-$, [**6**]$^-$ with each other reveals their similarity. On the other hand if the α and β values of [**4**]$^-$-[**6**]$^-$ are compared to the values of the corresponding phospha[1]ferrocenophane[25,26] derivatives, such as compounds **19** (P^{III}) and **20** (P^V), for which the α values are -26.9° and -25.4°, respectively (β values are 32.3° and 34.4°), large differences are found. The α for monoansa dimethylsilyl[1]cobaltabisdicarbollidephane [**21**]$^-$ is -6.8º, smaller than those found in [**4**]$^-$ - [**6**]$^-$.

As it would be expected, the effect of the chalcogen atom on the phosphorus does not affect significantly the geometrical parameters, only β and β' become slightly smaller as the covalent radius of the chalcogen is bigger. Of importance is the effect of the benzene-bridge in [**2**]$^-$ as it causes that α is +6.8º,[13b] being among the smallest angles reported to date for monoansa or diansa compounds. This clearly shows the synergistic effect of one ansa to the confronting one. For the monoansa metallacyclophanes ([**4**]$^-$, [**5**]$^-$, [**6**]$^-$) angle α is between -9.3 to -9.5º while the introduction of the confronting ansa moiety (compound [**7**]$^-$) causes a relaxation of the structure to an angle α of -3.8º. On the other hand in aromatic monoansa [**2**]$^{-}$[13b] and ethene monoansa [**22**]$^{-}$[27] ions the C_c-Co(III) distances are longer than in the corresponding diansa [**7**]$^-$ ion. It is possible then to summarize that a P bridge through C atoms shortens Co-C_c bonds whereas an aromatic monoansa bridge through B atoms elongates Co-C_c bonds. Angle δ is almost 180º for mono and diansa phospha[1]cobaltabisdicarbollidephanes while for phospha[1]ferrocenophane is 160º, much smaller given the higher distortion found on the latter.

Although some computational studies on the phosphorus–chalcogen bond were found in the literature,[28] few studies have been done on bulky phosphines or with strongly

electron-withdrawing groups bonded to phosphorus.[29] The nature of the phosphorus-chalcogen bonds of [**4**]$^-$-[**8**]$^-$ and phospha[1]ferrocenophane derivatives was determined by DFT calculations, natural bond orbital (NBO) analysis and quantum theory of atoms in molecules (QTAIM). The geometries of these derivatives were modelled by DFT calculations to have the full set of compounds. Previously, we explored the crystallographic entries in the Cambridge Data Base (CSD)[30] on monoansa and diansa cobaltabisdicarbollide anions that connect the dicarbollide units either through the two C_c atoms, the two B atoms or hybrid C_c and B atoms. Only a crystal structure (CSD code HOBFIO) of anionic monoansa cobaltabisdicarbollide through the C_c atoms showing a *meso* conformation has been found.[11b] When exploring the crystallographic entries of anionic monoansa cobaltabisdicarbollide through the B atoms nine crystal structures showing *meso* conformation have been found.[31] There is no crystal structure of diansa cobaltabisdicarbollide reported at the CSD. On the basis of this search and the crystal structures reported in this paper, all theoretical calculations have been done on the *racemic* form for the anionic monoansa phospha[1]cobaltabisdicarbollidephanes and on the *meso* form for the anionic diansa phospha[1]benzene[2]cobaltabisdicarbollidephanes. The resulting optimized geometries are given in Table 5. The good agreement between the calculated and crystallographic structural data establishes that the calculated compounds provide an accurate model for the geometrical study. It is worth to mention that phosphorus oxidation causes a decrease on α and an increase on β in both ferrocene and cobaltabisdicarbollide moieties. Finally, the diansa phospha[1]benzene[2]cobaltabisdicarbollidephanes is the first reported compound that as a result of having diansa confronted bridges cause a relaxation of the structure, mostly due to the compensation of both ansa elements, i. e.

α: +6.0º for [**2**]$^-$ and -5.8º for [**7**]$^-$. Experimental α values are +6.8º for [**2**]$^-$, and -3.8º for [**7**]$^-$.

When comparing the structures of phospha[1]ferrocenophanes and phospha[1]cobaltabisdicarbollidephanes we noticed that the former compounds, **19** and **20**, have distorted cyclopentadiene planes shown by the geometrical parameter α (–27.2º and –26.3º, respectively). In contrast, phospha[1]cobaltabisdicarbollidephanes ([**3**]$^-$-[**6**]$^-$) have less distorted C_2B_3 planes (-10.3º< α<-10.9º) and this is even more accentuated in the diansa phospha[1]benzene[2]cobaltabisdicarbollidephane [**7**]$^-$ and [**8**]$^-$ where the C_2B_3 planes are almost parallel (α= -5.8º). A geometrical consequence of the more pronounced tilting in phospha[1]ferrocenophanes than in phospha[1]cobaltabisdicarbollidephane is that the bridging phosphorus is closer to the sandwiched metal in the latter, even taking into account the relative cobalt and iron van der Waals radii. The crystal structure of [**7**]$^-$ shows a distance of 2.769(1) Å between Co and P that is smaller than sum of vdW radii.[32]

In order to probe the nature of intramolecular interactions, NBO analysis have been performed on anions [**3**]$^-$-[**8**]$^-$. By using the second order perturbation theory analysis included in NBO it is possible to estimate donor-acceptor interactions between natural bond orbitals, along with their energy. For non-oxidized monoansa [**3**]$^-$ and diansa [**7**]$^-$ anions three different interactions can be found between phosphorus and cobalt (Figure 11a). For [**3**]$^-$, two of them with an energy of 21 kcal·mol^{-1} correspond to the interactions between the electrons of the P-C_c bonds and the empty 4*s* orbital on cobalt. The third interaction is found between the lone pair on phosphorus and the same 4*s* orbital as before, with an energy of 10 kcal·mol^{-1}.

On the other hand, for oxidized anions [**4**]$^-$, [**5**]$^-$ and [**6**]$^-$ there is no interaction between phosphorus and cobalt due to the absence of the P lone pair, which is bonded to the

chalcogen atoms (Figure 12). The interactions found in these compounds are between the P-C_c bonds and the empty 4*s* orbital of cobalt with a similar energy of *ca.* 8 kcal·mol^{-1} independent of the chalcogen atom. Moreover, it is possible to find interactions of about 12-20 kcal·mol^{-1} between lone pairs on chalcogen and the P-C_c bond, leading to a decrease of the electronic density on the chalcogen. The energy of these interactions follow the tendency O>S>Se. Interactions between the P-C_c bonds and the B6/B6' vertices with an energy of *ca.* 7 kcal·mol^{-1} have also been observed. These interactions provide extra ways to give electronic density back to the metallacarborane cluster (see Table S.1. in Supporting Information for more details).

Finally, in order to prove the existence of a direct interaction between the Co and the P, an AIM (atoms in molecules) analysis on anions [**3**]$^-$ and [**4**]$^-$ was performed.[33] A critical point (3, +1) was identified between the Co and the P atoms in both anions indicating the centre of a ring rather than the existence of a direct interaction. Figure 11b shows a 2D representation of the NBO orbitals interaction between phosphorus and cobalt for [**3**]$^-$. Although the analysis have not led to the identification of a dative interaction (BCP), the existence of a critical ring point (RCP in this case) brought us to the hypothesis that an influence of the ansa is found on the metal center, and that this can happen on both sides of the metal, causing a synergistic effect of the diansa observed in the spectroscopic and electrochemical parameters as will be discussed in the next sections.

2. NMR spectral considerations.

NMR spectroscopy has been a useful tool for the characterization of boranes, carboranes and metallacarborane clusters for many years.[34] The sensitivity of the electron distribution in carboranes to the presence of substituents has long been

apparent.[35] However, only few computational analysis of the ^{11}B NMR chemical shifts for metallabisdicarbollide[36] and its derivatives[11b] have been reported and none on ^{31}P NMR of phosphines containing metallabisdicarbollide groups. With the aim to obtain an interpretation of the experimental ^{11}B NMR and ^{31}P spectra of these monoansa phospha[1]cobaltabisdicarbollidephane and diansa phospha[1]benzene[2]cobaltabisdicarbollidephane species, theoretical calculations of $\delta(^{11}B)$ and $\delta(^{31}P)$ values have been carried on several of the metallabisdicarbollide derivatives reported in this paper.

2.a. Comparison between ^{31}P NMR spectra of non-oxidized and oxidized species. In the majority of common ligands, the phosphinechalcogenide unit gives a signal to lower field than the parent phosphine.[37] In fact, this behaviour is common in most of phosphine molecules and it is interpreted due to an electron donation from phosphorus to chalcogen, causing a decrease in the electron density of the P. It is noticeable (Table 1) that the resonances of the P^{III} anions [**3**]$^-$, [**7**]$^-$, [**11**]$^-$ and [**15**]$^-$ appear at a very downfield chemical shift when compared with the anionic diphosphine [1,1'-$(PPh_2)_2$-3,3'-Co(1,2-$C_2B_9H_{10})_2$]$^-$ previously reported by our group and that showed resonances at 25 ppm.[38,29] This means that the electronic environment on phosphorus in the monoansa phospha[1]cobaltabisdicarbollidephanes or diansa phospha[1]benzene[2]cobaltabisdicarbollidephanes is remarkably different, suggesting that electron density from phosphorus is being shared with other parts in the molecule. In addition, once oxidized by chalcogenides (O, S and Se), most of the resonances appear at a higher field than these corresponding to the phosphine precursor (See Table 1). What is responsible for this behavior?.

It is known that *o*-carborane cluster is electron-withdrawing through the carbon atoms and, consequently, can deplete electron density on phosphorus.[39] This should influence

the ^{31}P chemical shift of the P atom ansa bonded to cobaltabisdicarbollide via the cluster carbon atoms, however no "abnormal" ^{31}P NMR were observed in our previously reported [1,1'-$(PR_2)_2$-3,3'-$Co(C_2B_9H_{10})$]$^-$ phosphane derivatives.[38] Therefore the "abnormal" ^{31}P NMR observed in monoansa phospha[1]cobaltabisdicarbollidephane and diansa phospha[1]benzene[2]cobaltabisdicarbollidephane has to be attributed to the small cycle generated and/or to the closeness of the Co via a Ligand-to-Metal Charge Transfer (LMCT). In the case of [n]ferrocenophanes, the ^{57}Fe Mössbauer spectra suggested the possibility of a dative interaction between the ansa element and the iron atom.[40,41] This had been observed for phosphorus, carbon, silicon, etc. even though the Fe···X distance was longer than the sum of the covalent radii,[28d] but shorter than the sum of the vdW radii.[32]

To interpret the "abnormal" ^{31}P NMR chemical shifts, the geometry optimizations indicated in the Structural Details section have been used. Then, a theoretical calculation of ^{31}P NMR chemical shifts taking PPh_3 as a reference has been made. The good agreement between the calculated and experimental chemical shifts provided a new evidence to prove that the optimized geometry is a good representation of the molecular structure in solution. Table 6 shows the calculated and experimental chemical shifts for compounds [**3**]$^-$, [**4**]$^-$, [**5**]$^-$, [**6**]$^-$, [**7**]$^-$ and [**8**]$^-$. The trend between computed and experimental values is in good agreement except for [**6**]$^-$ where the relativistic effect of the Se atom can be important. To rule out that the small cycle was the only influence, a phospha[1]cobaltabisdicarbollide geometrically similar non-metal containing rigid cyclophane, μ–P-biphenyl, was computationally studied along with its oxidized form (μ–P(O)-biphenyl). In this case, the calculated ^{31}P NMR chemical shifts follow a "normal" pattern: the oxidized species is more deshielded than the non-oxidized form.

Therefore, the presence of a metal centre near the phosphorus atom might be responsible for the higher than expected deshielding on the non-oxidized compounds.

These studies were complemented by calculation of the paramagnetic ($\Delta\sigma_p$) and diamagnetic ($\Delta\sigma_d$) contributions to the shielding constant for some oxidized and non-oxidized monoansa and diansa molecules. The results are shown in Table 7. There it may be observed that for the monoansa and diansa metallacyclophanes ([**3**]$^-$, [**4**]$^-$ [**7**]$^-$ and [**8**]$^-$) the $\Delta\sigma_d$ contribution has almost the same value for non-oxidized and oxidized species. It must be therefore the $\Delta\sigma_p$ contribution the major responsible for the ^{31}P NMR chemical shift. On the other hand, in the geometrically similar non-metal containing μ–P-biphenyl, the chemical shift is caused by both $\Delta(\sigma_d)$ that is 5.2 ppm and $\Delta(\sigma_p)$ that is 9.4 ppm. The diamagnetic contribution is mainly attributed to the electron density on the nucleus and this seems to be the same for monoansa [**3**]$^-$ and [**4**]$^-$ anions. Conversely, paramagnetic contribution is attributed to electron spins and on the interaction between occupied and unoccupied levels, respectively.[42] The rather large contribution of the lone pair on phosphorus in [**3**]$^-$ and [**7**]$^-$ on the highest occupied molecular orbital (HOMO) causes a larger paramagnetic contribution which is not found when those electrons are bonded to the calchogen atom ([**4**]$^-$ and [**8**]$^-$), where the HOMO is centered on the metal (Figure 13 and 14).

Throughout this paper we emphasize the synergistic effects of the confronting two ansa moieties. The ^{31}P NMR is another example. The experimental ^{31}P NMR of monoansa and diansa cobaltabisdicarbollidephanes are different, for [**3**]$^-$ is 71.1 whereas for [**7**]$^-$ is 73.2 ppm. On the contrary, their oxidized forms [**4**]$^-$ and [**8**]$^-$ display the ^{31}P NMR almost at the same $\delta(^{31}P)$, 33.7 and 33.5 ppm, respectively. These data suggest that when the lone pair on P is available for inner molecular use, there is synergy between

the two bridging units. When this lone pair is unavailable for inner use, as is the case when the P is oxidized, the synergy of the two bridging fragments is switched off.

2.b. Qualitative description of the ^{11}B NMR spectra chemical shift dependence.

In order to observe the effect of the P^{III} or P^{V} bridge on the $\delta(^{11}B)$ as well as on the paramagnetic and diamagnetic contributions to the ^{11}B NMR spectra of monoansa and diansa compounds, theoretical calculations have also been done. Figure 15 displays the calculated $\Delta\delta(^{11}B)$ resonances of [**3**]$^-$, [**4**]$^-$, [**7**]$^-$ and [**8**]$^-$ taking as references the chemical shifts of parent [**1**]$^-$ and [**2**]$^-$ species, respectively. The analysis of calculated $\delta(^{11}B)$ shows a different behavior for monoansa or diansa metallacyclophanes. While for the monoansa species the most affected vertices (B12 and B12') are the ones antipodal to the C_c-PR bonds, for the diansa compounds the largest difference in chemical shifts is seen on the vertices B7 and B7' at the C_2B_3 face.

The diamagnetic ($\Delta\sigma_d$) and paramagnetic ($\Delta\sigma_p$) contribution to the shielding differences in monoansa [**3**]$^-$, [**4**]$^-$ and diansa [**7**]$^-$, [**8**]$^-$ as referred to [**1**]$^-$ and [**2**]$^-$ respectively have been calculated (see Supporting Information for more details). For monoansa phospha[1]cobaltabisdicarbollide [**3**]$^-$ and [**4**]$^-$, the vertices B(12) and B(12') are the most affected by both contributions ($\Delta\sigma_d$ and $\Delta\sigma_p$). However, as they have opposite signs, $\Delta\sigma_p$ is the contribution that affects mostly the resonances on B(12) and B(12'). The same explanation is valid for diansa phospha[1]benzene[2]cobaltabisdicarbollide, [**7**]$^-$ and [**8**]$^-$.

3. Cyclic voltammogram studies.

With no debate, the archetype of the metallocenes is ferrocene. Unlike monoansa or diansa ferrocenophanes, that are invariably strained, the cobaltabisdicarbollide unit allows for unprecedented and relaxed confronting diansa sandwich complexes without

major perturbation of the original sandwich structure as seen at the structural section. Therefore the peculiar geometric characteristics of cobaltabisdicarbollide has permitted to combine in an unprecedented way a donor, D, (the PR bridge) and an acceptor, A, (the benzene brigde) in a confronting way (Figure 16). As a result, [**7**]$^-$ and [**15**]$^-$ are highly compact but relaxed phospha[1]benzene[2]cobaltabisdicarbollidephane species. Indeed these molecules do not allow for any degree of internal motion, with the possible exception of an inversion on P. No comparable example has been found in the literature for any metallocene. The more compact ones possible being the widely studied diansa-[2,3]ferrocenophanes with both trisulfide (or triselenide) and hydrocarbon bridges.[7]

In order to examine the effect of the D and A units on the $Co^{3+/2+}$ couple, the set of cobaltabisdicarbollide anions [**4**]$^-$, [**5**]$^-$, [**6**]$^-$, [**7**]$^-$, [**8**]$^-$, [**11**]$^-$, [**15**]$^-$ and [**16**]$^-$ was studied. All CVs of these compounds show one reversible redox wave that corresponds to the $Co^{3+/2+}$ redox couple, and this is the only wave discussed in this paper to study the influence of the donor and the acceptor bridges. The experimental $E_{1/2}$ values, refereed to *fc*, for the $Co^{3+/2+}$ couple for each anion are indicated in Table 9.

As Lever and co-workers reported,[43] an electrochemical parametrization in sandwich complexes of the first row transition metals can be established by assigning electrochemical parameters to the ligands. We will adhere to Lever's approach due to the sandwich nature of the cobaltabisdicarbollide anions. However, certain inaccuracies are expected because Lever's parametrization is generated from data obtained from organic ligands. For metal-centered redox reactions the following equation is applied:

$$E_{calc}(M^{n+1}/M^n) = S_M \Sigma E_L(L) + I_M \qquad \text{Equation 1}$$

The parameters S_M and I_M for a particular $M^{n+1/n}$ couple are constants. In organic solvents, for $Co^{3+/2+}$ are 0.83(0.05) and -1.16(0.13) V, and for $Fe^{3+/2+}$ are 0.99(0.00) and 0.00(0.01) V, respectively refereed to Standard Hydrogen Electrode (SHE).[43] Despite

the relatively large standard deviation SD, the fact that cobaltabisdicarbollide follows Equation 1 derived mostly from metallocenes, evidences that cobaltabisdicarbollide is a metallocene-like molecule that behaves as such. We have applied Equation 1 to calculate the E_L contribution of the ligand $[7,8\text{-}C_2B_9H_{11}]^{2-}$ that can be estimated as -0.00(0.10) taken the experimental $E_{1/2}$ value for $[3,3'Co\text{-}(1,2\text{-}C_2B_9H_{11})_2]^-$ obtained in this work. Likewise, E_L for phospha[1]cobaltabisdicarbollidephane [**3**]$^-$ is +0.22 V, whereas for benzene[2]cobaltabisdicarbollidephane [**2**]$^-$ is -0.35 V.

The diansa phospha[1]benzene[2]cobaltabisdicarbollidephane. Lever parameters have shown the redox ligand additivity in the $Co^{3+/2+}$ sandwich couple. A possibility existed that the opposing donor influence, D, of the –PR moiety and the acceptor influence, A, of the bridging benzene could in part cancel themselves. The effect of the benzene bridge was -0.35V, whereas the bridging PR was +0.16(0.01)V (R= Ph) and +0.22V (R= ^{t}Bu), both with regard to the parent [**1**]$^-$. The influence of the R group on monoansa phospha[1]cobaltabisdicarbollidephosphane was almost negligible at this stage. Therefore a simple addition of both the effect of the acceptor (benzene) and the effect of the donor (-PR), in similarity to Lever's parametrization, would result in a -0.15V shift. This was, however, not the case and the cooperative result of the synergy of the D and A moieties resulted in a +0.22V shift for R= Ph or a small -0.05V shift for R= ^{t}Bu. Interestingly, the once almost equal R effects (R= ^{t}Bu, Ph) in the monoansa phospha[1]cobaltabisdicarbollidephanes, become clearly distinct when the D and A synergy is put to work in the diansa phospha[1]benzene[2]cobaltabisdicarbollidephanes. The result of the synergy is not to cancel both effects but to stress the effect of one. For this confronting phospha[1]benzene[2]cobaltabisdicarbollidephane, the anodic shift of the P-R is the enhanced one.

Lowering the inner molecular availability of the lone pair on phosphorus. As the lone pair on P had been considered the basis for its D expected character, its lesser availability anticipated an alteration in the electronic density around the metal core, and therefore a modified $E_{1/2}(Co^{3+/2+})$ was predicted. To accomplish this objective, phospha[1]benzene[2]cobaltabisdicarbollidephanes [**7**]$^-$ and [**15**]$^-$ were taken to react with hydrogen peroxide and with sulfur to produce covalent P-O, compounds [**8**]$^-$ and [**16**]$^-$, and P-S bonds, compounds [**9**]$^-$ and [**17**]$^-$, respectively. The resulting oxidized molecule either with O or S preserved the original charge of the original phospha[1]benzene[2]cobaltabisdicarbollidephane. In both oxidations the $E_{1/2}(Co^{3+/2+})$ values shifted anodically, a precise 0.14V for O, the shift being independent of R. Therefore, the lesser availability of the lone pair even accentuated the anodic shift attributed to the P. It remained to be studied if this anodic shift was a consequence of the opposing effect of the bridging benzene, or conversely it was inherent to the bridging P-R moiety. To this aim, oxidation of phospha[1]cobaltabisdicarbollidephane, [**3**]$^-$, with H_2O_2 and sulfur was conducted to yield compounds [**4**]$^-$ and [**5**]$^-$, respectively. The $E_{1/2}(Co^{3+/2+})$ value has experienced a 0.21 V anodic shift, slightly more accentuated than with the additional presence of the benzene bridge. This indicates that the additional anodic shift of the $Co^{3+/2+}$ couple is largely due to the lesser availability of the lone pair on P, but attenuated by the synergist effect of the confronting second ansa, 0.21V *vs*. 0.14V.

4. UV-Visible spectrum.

Hawthorne and co-workers2[a] have reported that the UV-Visible spectra of [**1**]$^-$ in methanol consists of four absorptions at 216, 293, 345 and 445 nm, which is grossly in agreement with this reported later by Matel and co-workers[44] with one absorption band

(λ_{max} at 287 nm, $\varepsilon \approx 30.000$ l cm^{-1} mol^{-1}). The visible spectrum was interpreted by Cerný and co-workers[45] on the basis of the Ligand Field Theory. We recorded the UV-Visible spectra of [**1**]$^-$ in acetonitrile,[8,11] as this is the solvent used in the cyclic voltammetry studies, and although the spectrum was rather similar to these already reported, discrepancies exist in the λ positions and the absorption coefficients which indicate that these values are dependent on how the absorption (A) was measured.

We have recorded the UV/Vis spectrum of [**2**]$^-$, [**3**]$^-$, [**4**]$^-$, [**5**]$^-$, [**7**]$^-$, [**8**]$^-$, [**11**]$^-$, [**15**]$^-$ and [**16**]$^-$ in acetonitrile. The spectra did not show in general well defined peaks, which made it difficult to comparing them. To overcome this problem, a deconvolution in gaussian-type peaks was performed using line-fitting analysis. The goodness-of-fit (R^2) of all the spectra was between 0.999 and 0.996. The full set of data is shown in Table 8.

The results obtained for the parent compound [**1**]$^-$, as well as for the species [**3**]$^-$, [**4**]$^-$ and [**5**]$^-$ as representative examples are shown in Figure 17. As can be seen there, the deconvolution in Gaussians permitted discernment of the sub-band positions and the retrieval of λ_{max} that would otherwise have been impossible. Therefore, relevant comparisons can be made. It can be observed that absorptions near 220, 281, 329 and 445 nm, present in the spectrum of [**1**]$^-$, are indeed present in all the spectra with comparable λ values. These absorptions can then be attributed to the [3,3'-Co(1,2-$C_2B_9H_{11})_2$]$^-$ moiety. The benzene bridged cobaltabisdicarbollidephane, [**2**]$^-$, displays absorptions at 216, 236, 263, 275, 285, 297, 334 and 517 nm. These at 216, 285, 334 and 517 are almost coincident with the absorptions due to [**1**]$^-$. Therefore the set of absorptions at 236, 263 and 275 nm can be ascribed to the benzene bridge as they are also observed in *o*-xylene.[46] These absorptions are present in all the remaining benzene bridged cobaltabisdicarbollidephanes. It is of notice that the absorption near 240 nm observed in [**7**]$^-$ and [**8**]$^-$ is not found in [**15**]$^-$ and [**16**]$^-$. The last two do not have the P-

Ph moiety but the P^{t}Bu, which would suggest that the –P*Ph* moiety also contributes, or in some cases is the only responsible for the absorptions near 240 nm. We have ruled out that the lone pair on P plays a role in this absorption as PR_3 (R= alkyl) do not absorb above 200 nm. The column headed by 329 nm in Table 8 does not contain any void. This suggests that this absorption can be assigned to the cobaltabisdicarbollide fragment, however the two neighbouring columns are complementary. The voids in the left column are filled in the right column, and vice versa. It is relevant to indicate that with no exception the compounds having the absorptions near 370 nm are the diansa metallacyclophanes. Presumably, this band can be diagnosis for a synergistic effect between the two bridging units. In support of this is the difference of 20 nm in the column headed by 445 nm between the oxidized and non-oxidized phosphorus in [**7**]$^-$ /[**8**]$^-$ and [**15**]$^-$/[**16**]$^-$, whereas this difference is not observed for the [**3**]$^-$/[**4**]$^-$ couple. Additionally, a change on the d-d band of around 20 nm is also observed for [**3**]$^-$/[**7**]$^-$ and [**11**]$^-$/[**15**]$^-$ that can be attributed to the inclusion of the second ansa moiety, the boron-bridged aromatic ring.

To interpret the former results, HOMO and LUMO orbitals for [**3**]$^-$, [**4**]$^-$, [**7**]$^-$ and [**8**]$^-$ have been compared. These frontier orbitals are shown in Figures 13 and 14. Some observations can be drawn from these figures, a straightforward one is that the contribution of phosphorus to the HOMO of [**3**]$^-$ is very important, while for [**4**]$^-$ is inexistent. This agrees with the results obtained both for the NBO analysis and the ^{31}P NMR. The delocalization of the HOMO between the P and the Co ensures an electronic communication between these atoms through the cluster C_c atoms, that also contribute to the HOMO. These data parallel the results of the NBO analysis. As expected for the oxidized phosphine, in [**4**]$^-$ the phosphorus does not contribute to the HOMO orbital, mostly constituted by a *d* orbital on cobalt. For diansa metallacyclophanes [**7**]$^-$ and [**8**]$^-$,

the largest fragment contribution to the HOMO is due to the benzene bridging moiety; the lone pair in [**7**]$^-$ also contributes to the HOMO but its participation is much less than in [**3**]$^-$. No P contribution to the HOMO occurs in [**8**]$^-$. Of notice is the difference in $\Delta(E_{LUMO}-E_{HOMO})$ for monoansa [**3**]$^-$ and [**4**]$^-$ that is 0.19 eV and the diansa [**7**]$^-$ and [**8**]$^-$ that is 0.03 eV as can be deduced in Table 10. The smaller $\Delta\Delta(E_{LUMO}-E_{HOMO})$ for [**7**]$^-$ and [**8**]$^-$ has to be related to the synergistic effect of both ansa fragments discussed throughout the paper. The former values correlate with the electrochemical $E_{1/2}$ data shown in Table 9. While the $\Delta E_{1/2}$([**4**]$^-$/[**3**]$^-$) is 0.21V, the $\Delta E_{1/2}$([**8**]$^-$/[**7**]$^-$) is 0.14V.

All LUMO orbitals are metal-centered and all look very similar. The LUMO energies of the mono and diansa are very similar, thus demonstrating that the synergistic effect or, more specifically, the lone pair influence is solely based on the HOMO orbitals.

The changes on the d-d transition band are related to the HOMO and LUMO energies that depend on the electronic environment around the metal centre. The increasing easiness to reduce the cobalt atom in moving from [**1**]$^-$ to [**3**]$^-$ to [**4**]$^-$ as a result of the donor ability of the phosphine ligand is, however, not observed as a shift of this band on these monoansa cobaltabisdicarbollidephanes. On the other hand, for diansa metallacyclophanes [**2**]$^-$/[**7**]$^-$/[**8**]$^-$ a blue shift is observed from 517 to 460 nm, respectively. This shift is also observed on the E_{LUMO} as this energy is related to easiness to reduce the metal centre according to Koopman's theorem. In Table 10 it can be seen a summary of E_{HOMO}, E_{LUMO} and $\Delta E_{(HOMO-LUMO)}$ for selected compounds. The effect of the substituent on the phosphorus atom (Ph or ^{t}Bu) is negligible on the UV/vis spectra and also on their orbital energies. Looking at the $\Delta E_{(HOMO-LUMO)}$ it can be observed the dramatic effect of the aromatic B-bridge unit as it lowers the energy difference 1 eV. On the contrary, the donor ability of the phosphine ligand is observed

on the E_{LUMO} which decreases as it goes from [**1**]$^-$ to [**3**]$^-$ and [**4**]$^-$, and also from [**2**]$^-$ to [**7**]$^-$ and [**8**]$^-$.

Conclusions

The first highly compact diansa metallacyclophane has been prepared in which the two ansa units are not adjacent. The central core is the sandwich $[Co(C_2B_9H_{11})_2]^-$ and two rigid non-adjacent handles, one single P and two adjacent carbon atoms of a benzene ring, complete the molecule that has the shape of an amphora. The different nature of the two handles, geometrically placed in a confronting disposition, results in a donor and acceptor system with a redox electroactive core. The synergy of the two handles is reflected in every aspect of the molecule, including structure, electronic and spectroscopic properties, and redox activity. For instance, the confronted disposition of the two handles permits that the two "C_2B_3" cobalt coordinating planes to be quasi parallel, with almost no distortion relative to pristine $[Co(C_2B_9H_{11})_2]^-$. Contrarily, a noticeable deviation from the latter is found with the monoansa either phosphane [**3**]$^-$ or benzene precursor [**2**]$^-$. Another example of the synergy of the two handles is found in the redox activity of the $Co^{3+/2+}$ couple: the combined effect of the two handles shifts the $E_{1/2}$ to an E value that is not the simple addition of the two individual effects: one of them is clearly enhanced. Very important is the role of the phosphorus lone pair. When available the lone pair does participate in the electronic communication between the two handles through the redox electroactive site. This communication is blocked when the phosphorus lone pair is used for other activities outside the amphora molecule, e.g. when it is used to generate a P-E bond, E= O, S or Se. We expect that the geometrical, electronic and electrochemical properties of these robust and compact amphora-like diansa molecules will contribute to the generation of a new set of molecular functional

materials for applications in molecular electronics, sensors, and light harvesting among others.

Supporting material available:

Experimental section with full characterization of the synthesized compounds can be found in the Supporting Information. Calculation details are detailed!!!!!!!! Plots of calculated ^{11}B NMR diamagnetic (Figure S.1.) and paramagnetic (Figure S.2.) shielding constant differences in [**3**]$^-$ and [**4**]$^-$ as well as [**7**]$^-$ and [**8**]$^-$ referred to [**1**]$^-$ and [**2**]$^-$ respectively. Second order delocalization energies for the electron lone pairs and NBOs antibonding interactions for some monoansa and diansa phosphacobaltabisdicarbollidephanes (Table S.1). The crystallographic data for tetramethylammonium salts of compounds [**4**]$^-$ - [**7**]$^-$ can be obtained free of charge via www.ccdc.cam.ac.uk/conts/retrieving.html (or from the Cambridge Crystallographic Data Centre, 12 Union Road, Cambridge CB2 1EZ, U.K.; fax: (+44) 1223-336033; or e-mail: deposit@ccdc.cam.ac.uk). This material is available free of charge via the Internet at http://pubs.acs.org.

Acknowledgement

This work was supported by Spanish Ministerio de Ciencia e Innovación (CTQ2010-16237), CSIC (I3P grant to P.F.) and the Generalitat de Catalunya 2009/SGR/00279. The access to the computational facilities of High Performance Computing Centre of CSIC and Centre de Supercomputació de Catalunya (CESCA) is gratefully acknowledged.

Chart 1.- Schematic representation of diansa confronted and diansa adjacent metallocenophanes.

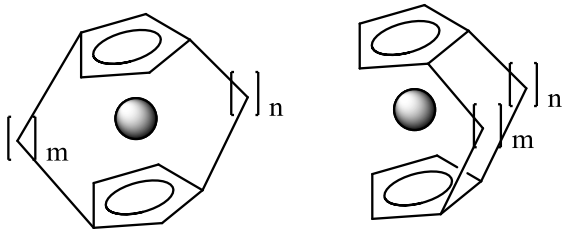

Diansa confronted [m][n]metallocenophane

Diansa adjacent [m][n]metallocenophane

Chart 2.- Schematic drawings of monoansa and diansa [**3**]$^-$-[**18**]$^-$ anions with reference compounds [**19**]-[**22**]$^-$.

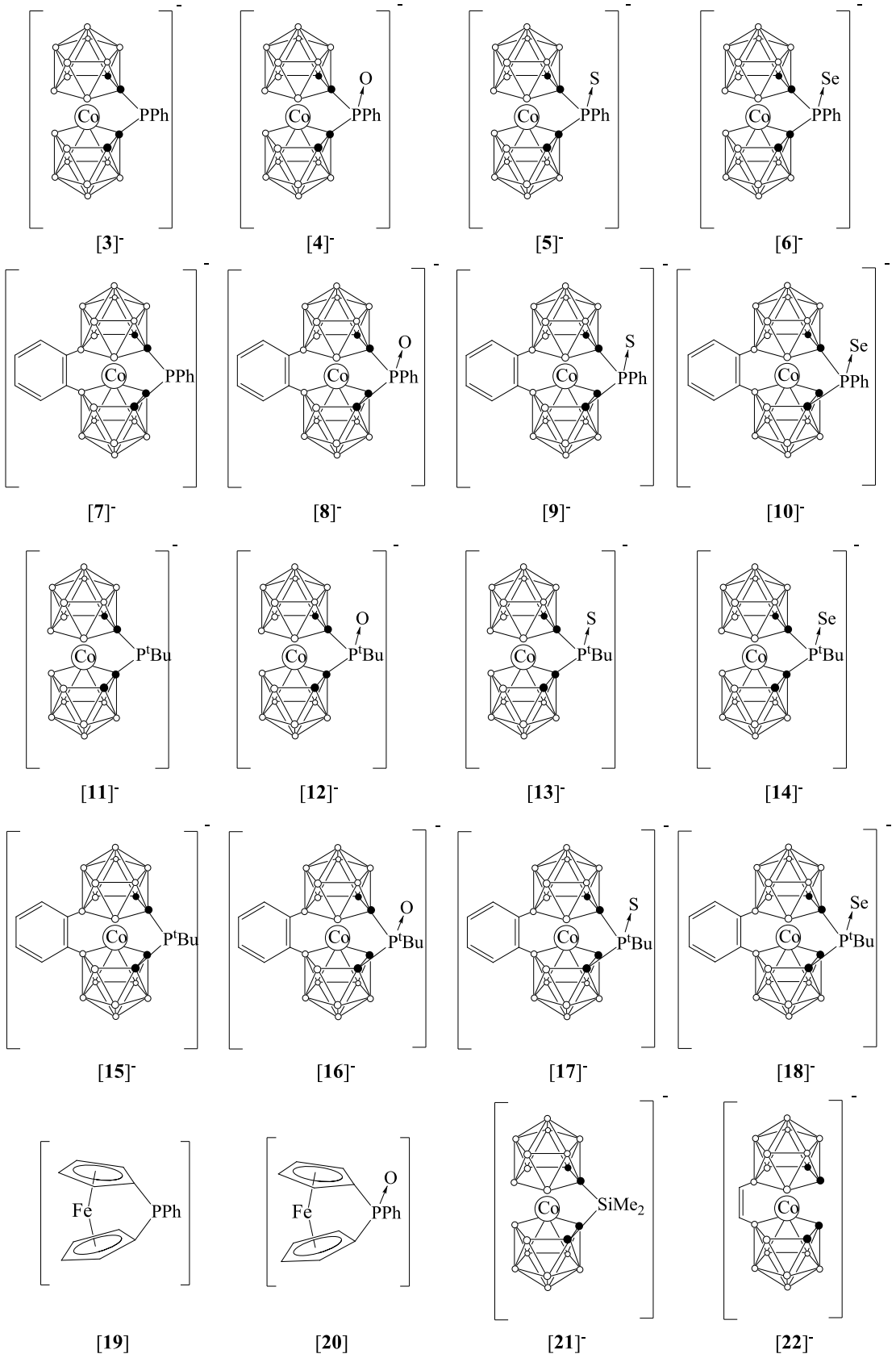

[**3**]$^-$ [**4**]$^-$ [**5**]$^-$ [**6**]$^-$

[**7**]$^-$ [**8**]$^-$ [**9**]$^-$ [**10**]$^-$

[**11**]$^-$ [**12**]$^-$ [**13**]$^-$ [**14**]$^-$

[**15**]$^-$ [**16**]$^-$ [**17**]$^-$ [**18**]$^-$

[**19**] [**20**] [**21**]$^-$ [**22**]$^-$

Scheme 1. Synthetic procedure for the preparation of bridged-phosphorus derivatives of [**1**]$^-$ and [**2**]$^-$.

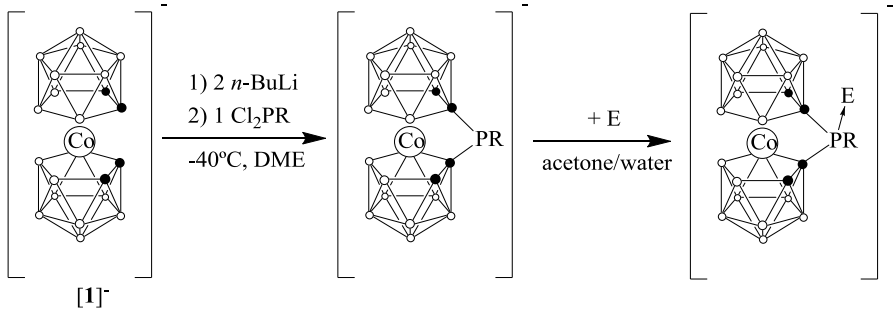

[**1**]$^-$

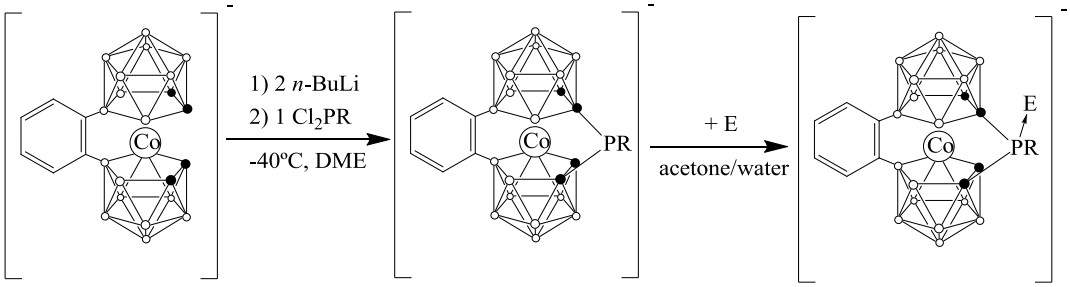

[**2**]$^-$

FIGURES CAPTION

Figure 1. Geometric isomers of the anionic monoansa metallacyclophosphanes [**3**]$^-$ and [**11**]$^-$ (view from the top of the pentagonal faces).

Figure 2. Geometric isomers of the anionic diansa metallacyclophosphanes [**7**]$^-$ and [**15**]$^-$ (view from the top of the pentagonal faces).

Figure 3. Experimental $^{11}B\{^1H\}$ NMR spectrum of Cs[**1**] (a), [NMe_4][**3**] (b) and [NMe_4][**4**] (c).

Figure 4. Experimental $^{11}B\{^1H\}$ NMR spectrum of Cs[**2**] (a), [NMe_4][**7**] (b) and [NMe_4][**8**] (c).

Figure 5. Molecular structure of [NMe_4]**7**·0.8CH_2Cl_2. (a) The structure with dichloromethane molecule. (b) The structure without dichloromethane molecule. (c) The top view of the situation in the asymmetric unit (P1a has a population of 0.8 and P1b 0.2). The thermal ellipsoids are set at 30% probability.

Figure 6. Molecular structure of [NMe_4][**4**]. The thermal ellipsoids are set at 15% probability.

Figure 7. Molecular structure of [NMe_4][**5**]. The thermal ellipsoids are set at 15% probability. [NMe_4]$^+$ has been omitted for clarity.

Figure 8. Molecular structure of [NMe_4][**6**]. The thermal ellipsoids are set at 15% probability. [NMe_4]$^+$ has been omitted for clarity.

Figure 9. (a) Structural features as a result of the strain induced by the phospha-bridge. (b) Schematic drawing of the diansa phospha[1]benzene[2]-cobaltabisdicarbollidephosphane units. D= donor group; A= acceptor group.

Figure 10. (a) Graphical representation of the interactions found in monoansa [**3**]$^-$ and diansa [**7**]$^-$ anions. (b) 2D plot of the NBO orbitals of monoansa [**3**]$^-$ corresponding to the interaction P-Co. The plane contains Co1-C2-P3 atoms.

Figure 11. Graphical representation of the interactions found in the oxidized monoansa [**4**]$^-$ and diansa [**8**]$^-$ anions.

Figure 12. HOMO (a) and LUMO (b) orbitals of monoansa anions [**3**]$^-$ (left) and [**4**]$^-$ (right).

Figure 13. HOMO (a) and LUMO (b) orbitals of diansa anions [**7**]$^-$ (left) and [**8**]$^-$ (right).

Figure 14. Plots of calculated ^{11}B NMR chemical shifts differences in [**3**]$^-$ (■) and [**4**]$^-$ (▲) as referred to [**1**]$^-$: the dashed line at zero corresponds to the chemical shift in [**1**]$^-$: ■ and ▲ correspond to δ([**3**]$^-$)-δ([**1**]$^-$) and δ([**4**]$^-$)-δ([**1**]$^-$), respectively. Plot below corresponds to [**7**]$^-$ (X) and [**8**]$^-$ (○) as referred to [**2**]$^-$ (pointed line).

Figure 15. UV/Vis spectra (solid lines) of some selected compounds, from top to bottom [**1**]$^-$, [**3**]$^-$, [**4**]$^-$ and [**5**]$^-$, and the results of line fitting with gaussians (dashed lines). The expanded sections on the right show the absorption near 450 nm amplified 20 times.

Figure 1. Geometric isomers of the anionic monoansa metallacyclophosphanes [**3**]$^-$ and [**11**]$^-$ (view from the top of the pentagonal faces).

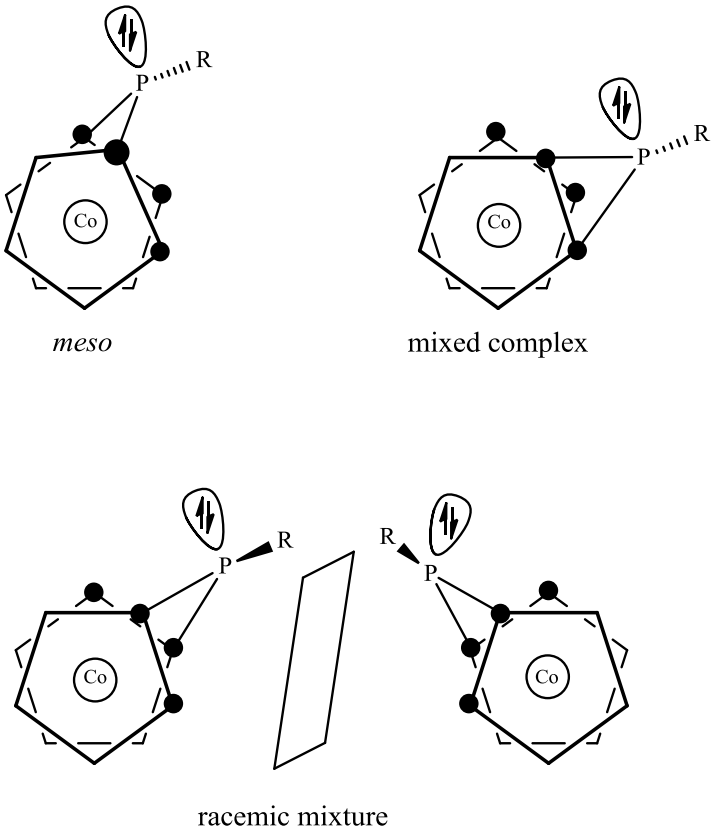

Figure 2. Geometric isomers of the anionic diansa metallacyclophosphanes [**7**]$^-$ and [**15**]$^-$ (view from the top of the pentagonal faces).

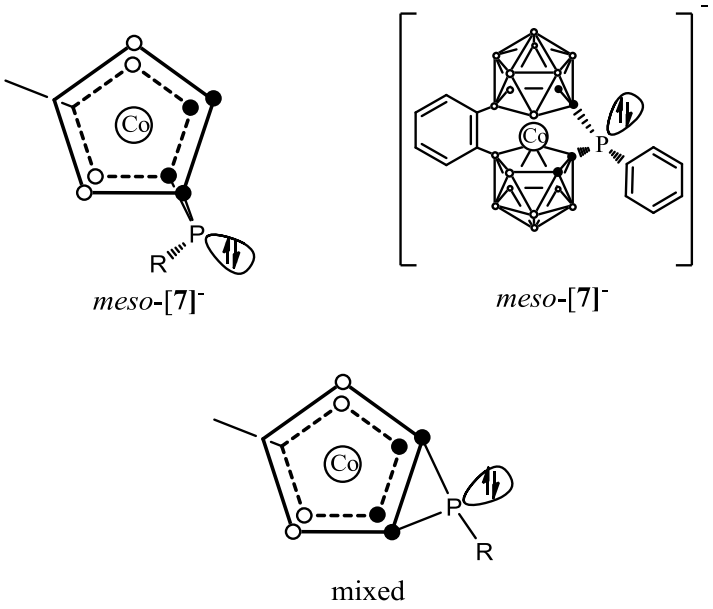

meso-[**7**]$^-$ *meso*-[**7**]$^-$

mixed

Figure 3. Experimental $^{11}B\{^{1}H\}$ NMR spectra of Cs[**1**] (a), $[N(CH_3)_4]$[**3**] (b) and $[N(CH_3)_4]$[**4**] (c).

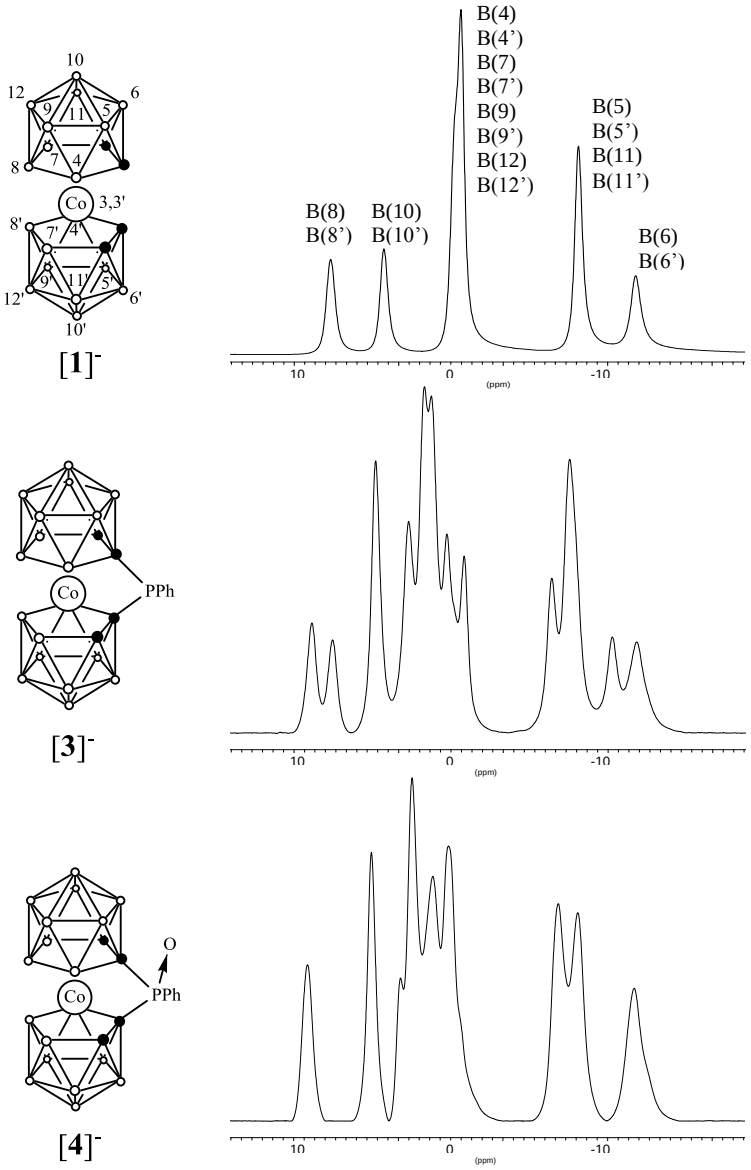

Figure 4. Experimental $^{11}B\{^1H\}$ NMR spectrum of Cs[**2**] (a), $[N(CH_3)_4]$[**7**] (b) and $[N(CH_3)_4]$[**8**] (c).

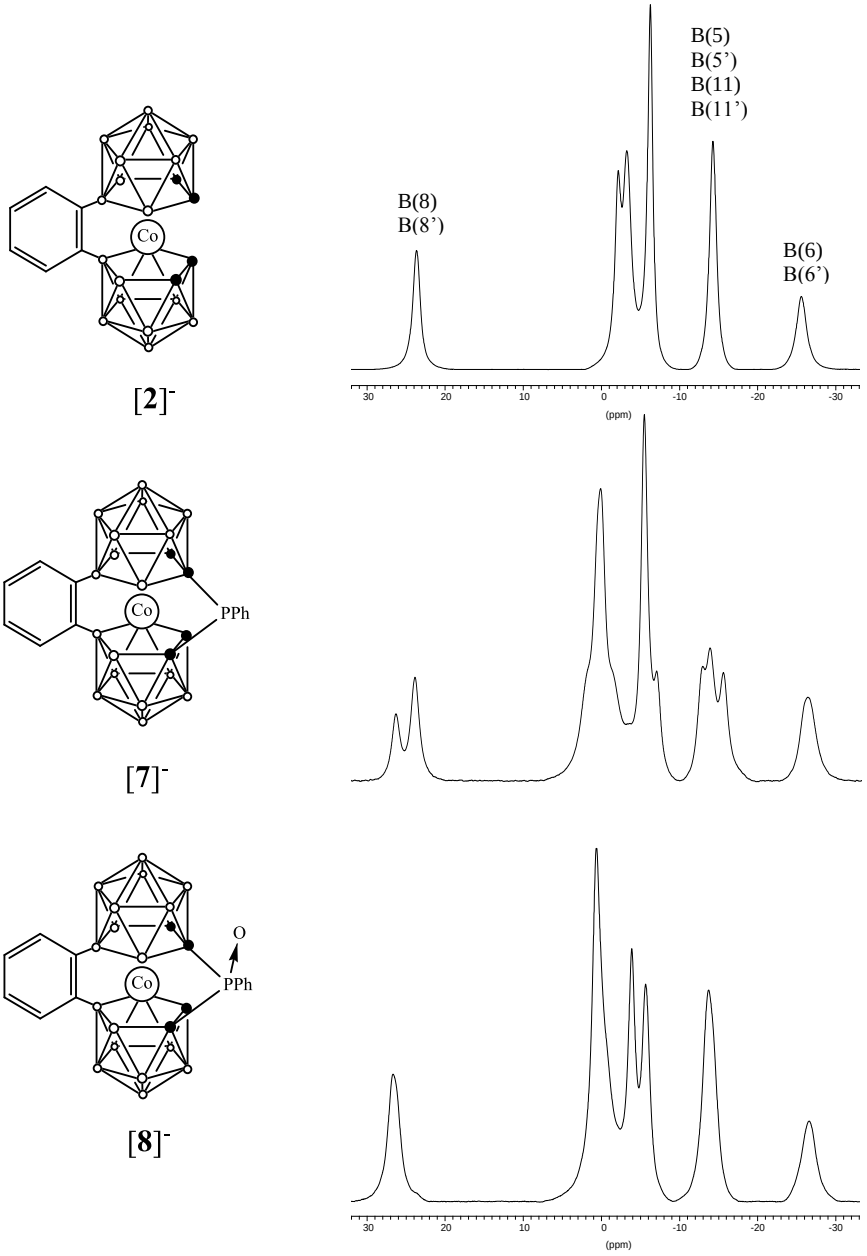

Figure 5. Molecular structure of $[NMe_4][\mathbf{7}]\cdot 0.8CH_2Cl_2$. (a) The structure with dichloromethane molecule. (b) The structure without dichloromethane molecule. (c) The top view of the situation in the asymmetric unit (P1a has a population of 0.8 and P1b 0.2). The thermal ellipsoids are set at 30% probability.

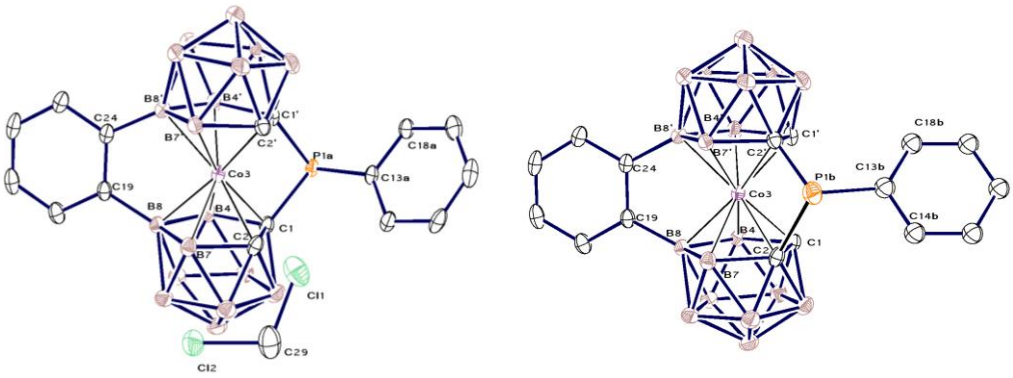

a) b)

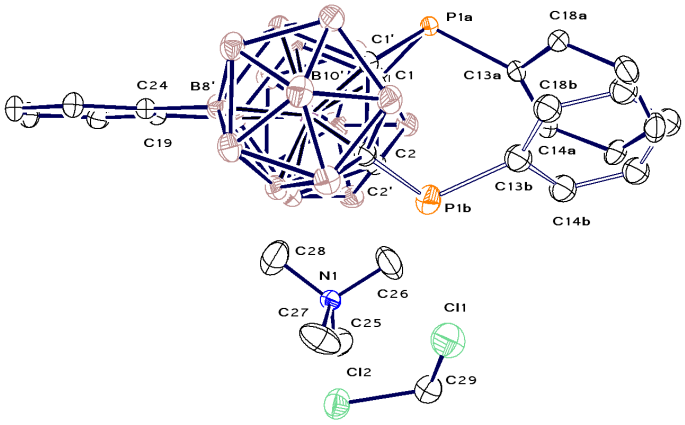

c)

Figure 6. Molecular structure of [NMe_4][**4**]. The thermal ellipsoids are set at 15% probability.

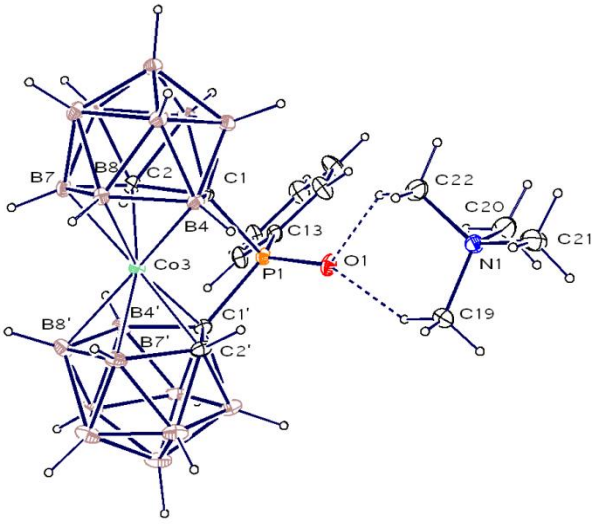

Figure 7. Molecular structure of $[NMe_4][\mathbf{5}]$. The thermal ellipsoids are set at 15% probability. $[NMe_4]^+$ has been omitted for clarity.

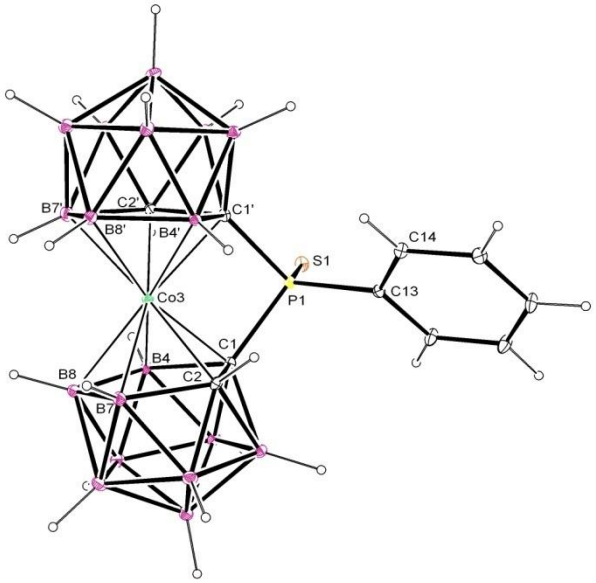

Figure 8. Molecular structure of $[NMe_4][\mathbf{6}]$. The thermal ellipsoids are set at 15% probability. $[NMe_4]^+$ has been omitted for clarity.

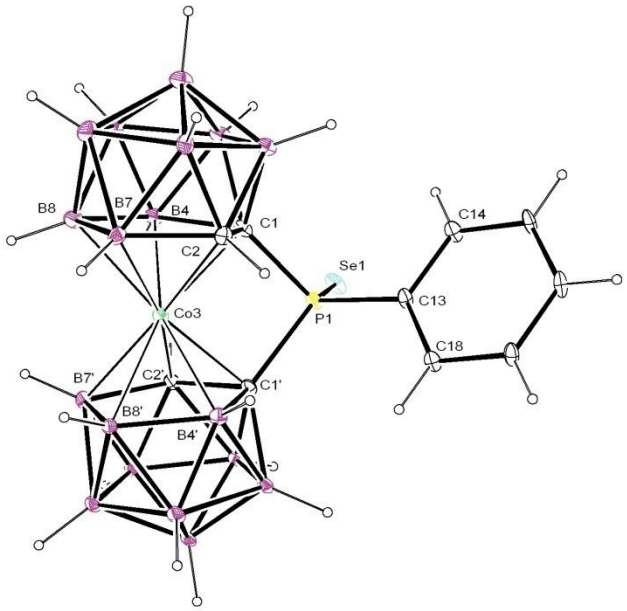

Figure 9. (a) Structural features as a result of the strain induced by the phospha-bridge. (b) Schematic drawing of the diansa phospha[1]benzene[2]-cobaltabisdicarbollidephosphane units. D= donor group; A= acceptor group.

(a)

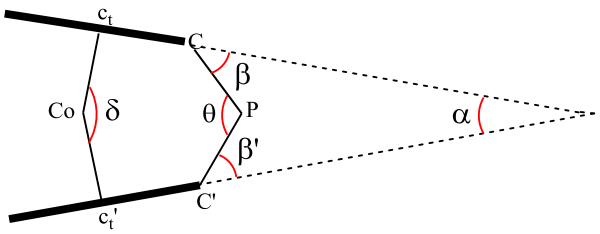

c_t = centroid by atoms C1, C2, B4, B7 and B8
c'_t = centroid by atoms C1', C2', B4', B7' and B8'

(b)

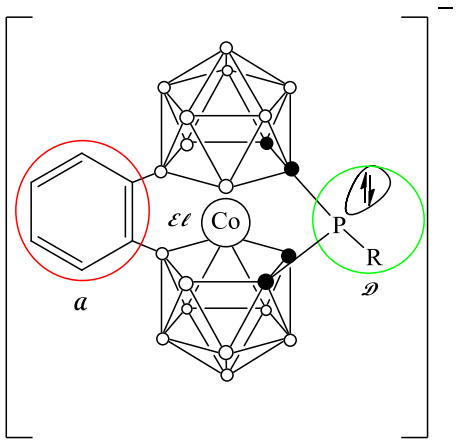

Figure 10. (a) Graphical representation of the interactions found in monoansa [**3**]$^-$ and diansa [**7**]$^-$ anions. (b) 2D plot of the NBO orbitals of monoansa [**3**]$^-$ corresponding to the interaction P-Co. The plane contains Co1-C2-P3 atoms.

a)

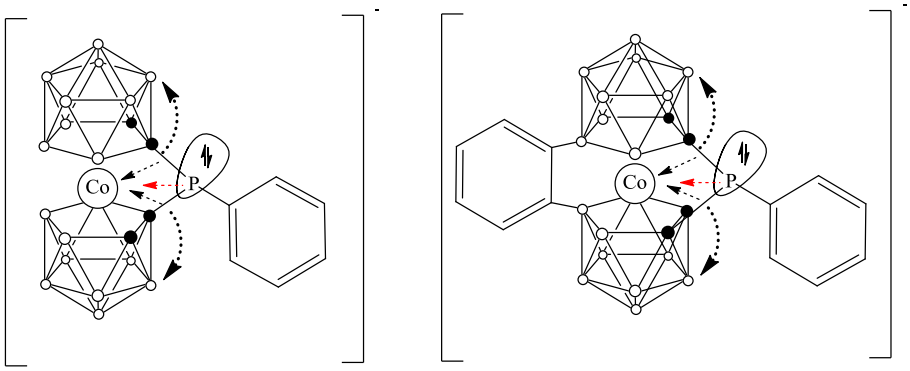

[**3**]$^-$ [**7**]$^-$

b)

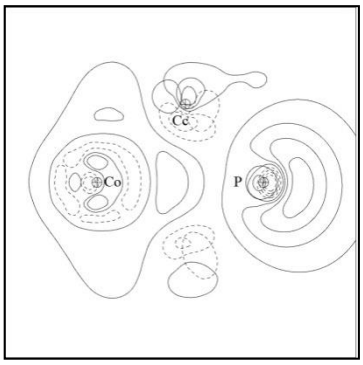

Figure 11. Graphical representation of the interactions found in the oxidized monoansa [**4**]$^-$ and diansa [**8**]$^-$ anions.

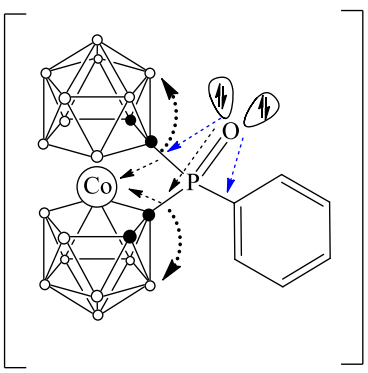

[**4**]$^-$

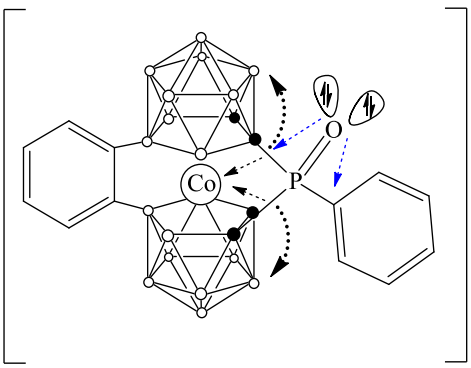

[**8**]$^-$

.

Figure 12. HOMO (a) and LUMO (b) orbitals of monoansa anions [**3**]$^-$ (left) and [**4**]$^-$ (right).

a)

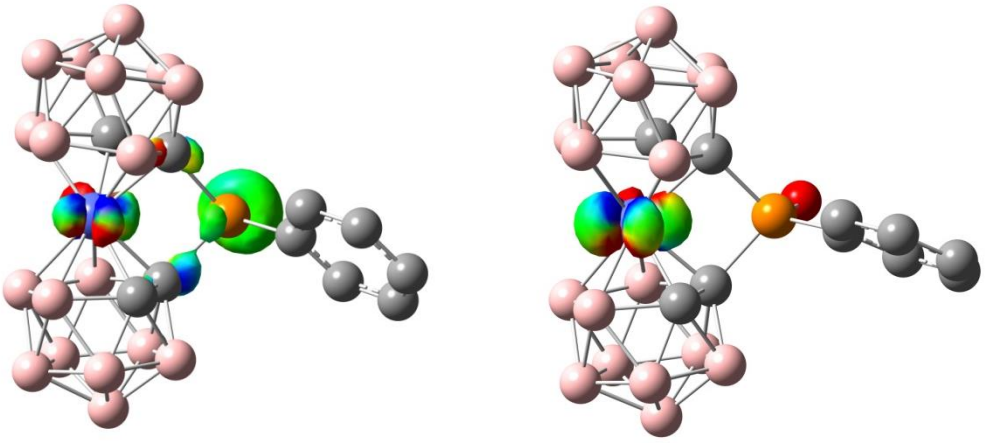

b)

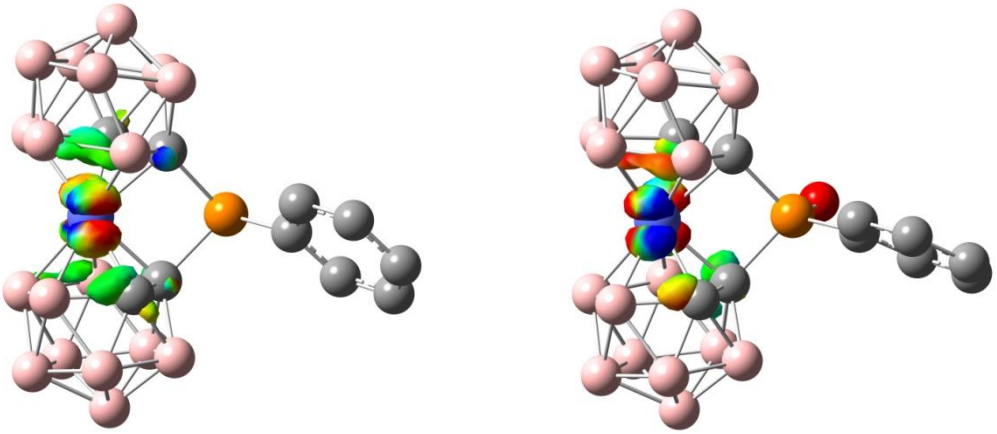

Figure 13. HOMO (a) and LUMO (b) orbitals of diansa anions [**7**]$^-$ (left) and [**8**]$^-$ (right).

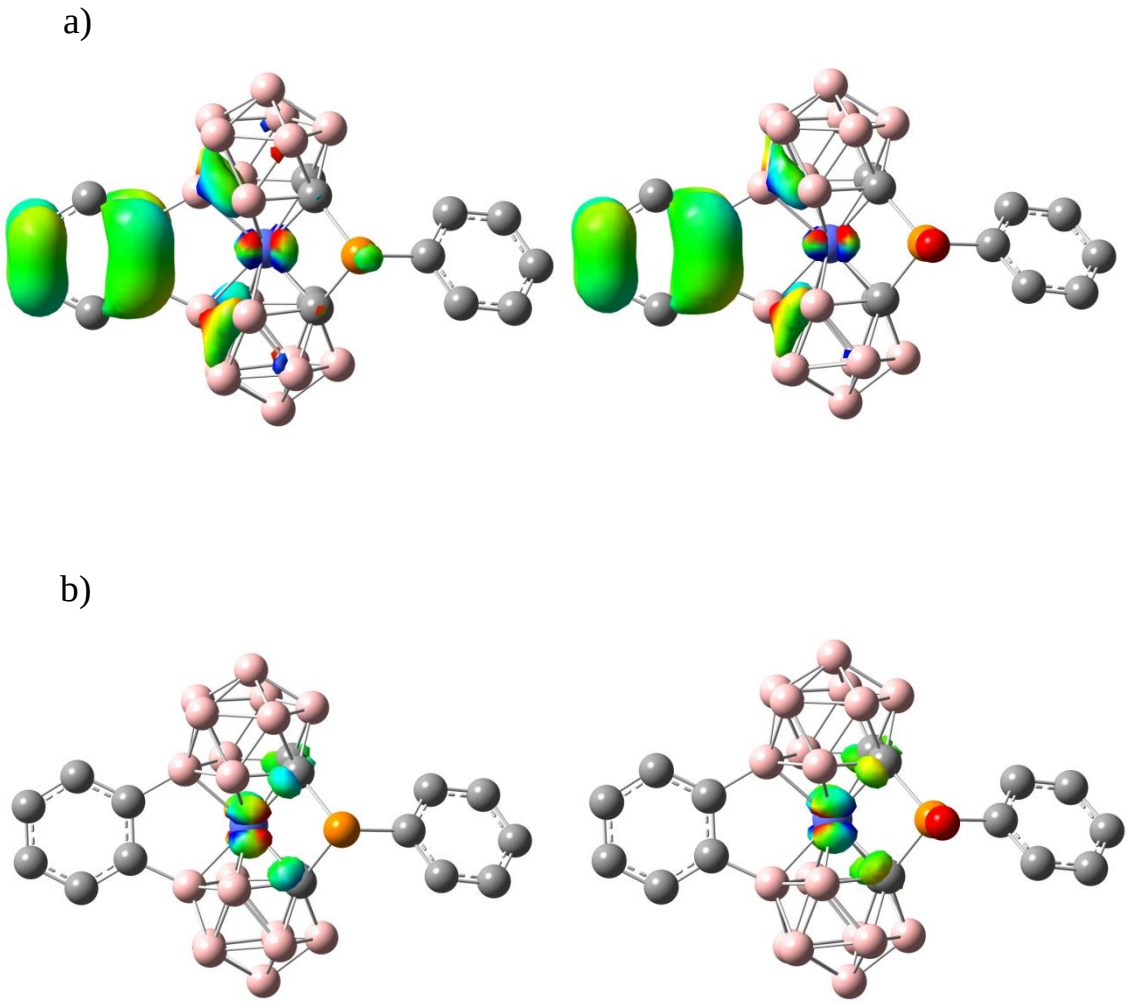

Figure 14. Plots of calculated ^{11}B NMR chemical shifts differences in [**3**]$^-$ (■) and [**4**]$^-$ (▲) as referred to [**1**]$^-$: the dashed line at zero corresponds to the chemical shift in [**1**]$^-$: ■ and ▲ correspond to δ([**3**]$^-$)-δ([**1**]$^-$) and δ([**4**]$^-$)-δ([**1**]$^-$), respectively. Plot below corresponds to [**7**]$^-$ (X) and [**8**]$^-$ (○) as referred to [**2**]$^-$ (pointed line).

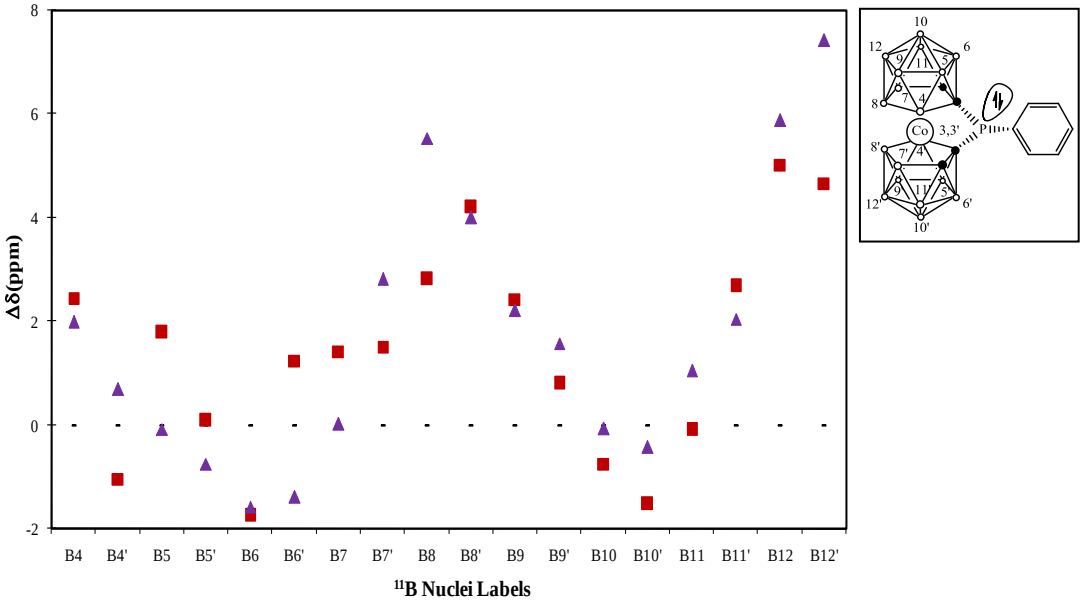

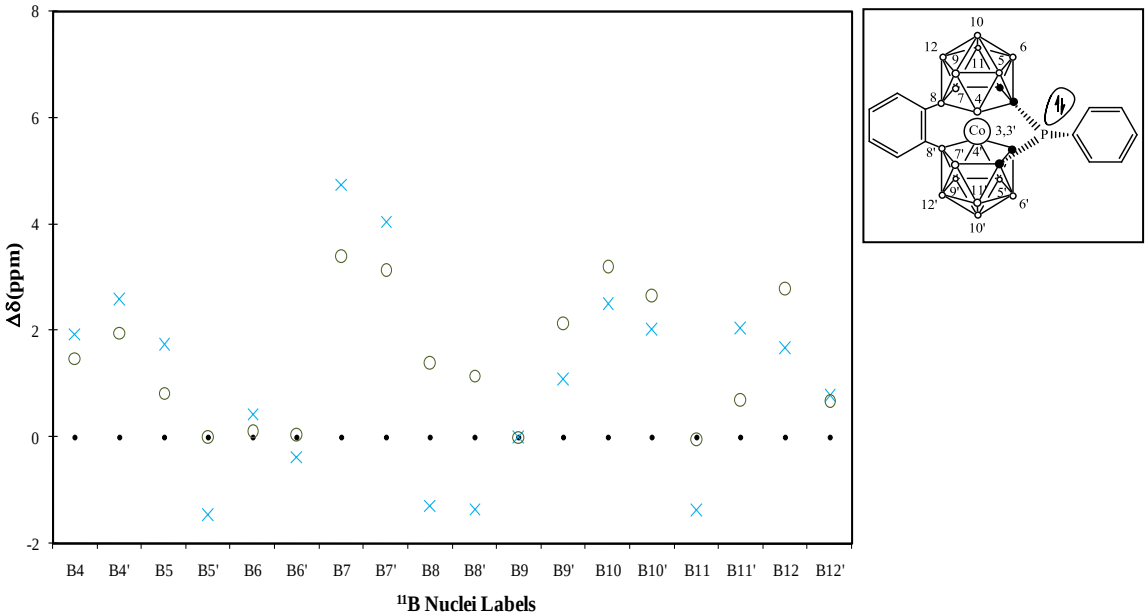

Figure 15. UV/Vis spectra (solid lines) of some selected compounds, from top to bottom [**1**]$^-$, [**3**]$^-$, [**4**]$^-$ and [**5**]$^-$, and the results of line fitting with gaussians (dashed lines). The expanded sections on the right show the absorption near 450 nm amplified 20 times.

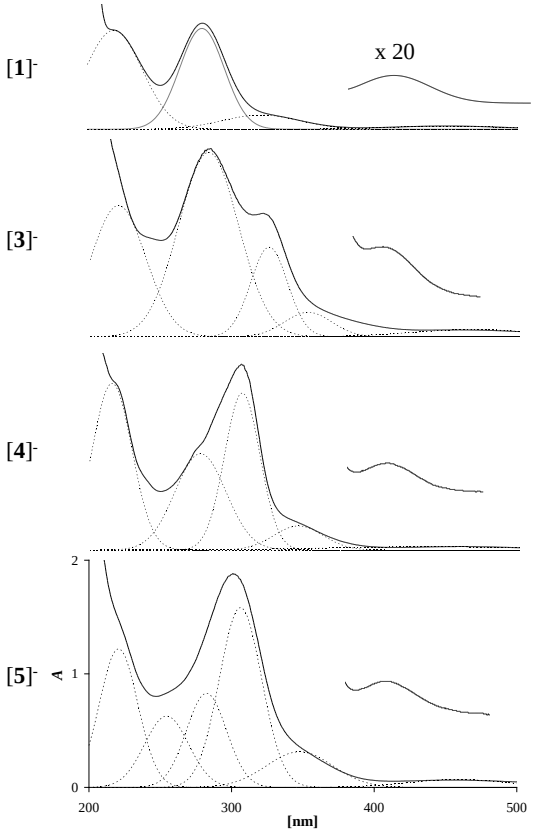

Table 1. Summary of ^{31}P NMR resonances of anions [**3**]$^-$, [**7**]$^-$, [**11**]$^-$ and [**15**]$^-$ and their corresponding oxidized compounds.

Table 2. Summary of crystallographic data for $[NMe_4]^+$ salts of [**4**]$^-$, [**5**]$^-$, [**6**]$^-$ and [**7**]$^-$.

Table 3. Selected bond lengths (Å) and angles (°) for the anions **[4]$^-$ – [7]$^-$**.

Table 4. Selected Structural Data for the $[NMe_4]^+$ salts of the studied compounds in comparison with phospha[1]ferrocenophanes ([**19**] and [**20**]). Also data for ions [**21**]$^-$, [**2**]$^-$ and [**22**]$^-$ are included.

Table 5. Selected Angles and Distances for the calculated compounds in comparison with calculated phospha[1]ferrocenophanes ([**19**] and [**20**]).

Table 6. Calculated and experimental ^{31}P NMR chemical shifts for several monoansa and diansa derivatives. Two bridge compounds (μ-P-biphenyl and μ-P(O)-biphenyl) without a metal are included as a comparison.

Table 7. Calculated diamagnetic and paramagnetic contributions to the ^{31}P NMR for several monoansa and diansa derivatives. Two bridge compounds (μ-P-biphenyl and μ-P(O)-biphenyl) without a metal are included as a comparison.

Table 8. UV/Vis spectra for compounds [**1**]$^-$, [**2**]$^-$, [**3**]$^-$, [**4**]$^-$, [**5**]$^-$, [**7**]$^-$, [**8**]$^-$, [**11**]$^-$, [**15**]$^-$ and [**16**]$^-$ in acetronitrile. λ positions [nm] and ε values [$L \cdot cm^{-1} \cdot mol^{-1}$] are reported and were calculated following line-fitting analysis.

Table 9. Calculated NPA charges on cobalt, cluster total charge (CTC), energy values (in eV) of the HOMO and LUMO orbitals, their energy difference and experimental $E_{1/2}$ [V/ *fc*] for several monoansa and diansa metallacyclophanes.

Table 1. Summary of ^{31}P NMR resonances of anions [**3**]$^-$, [**7**]$^-$, [**11**]$^-$ and [**15**]$^-$ and their corresponding oxidized compounds.

Compounds P(III)	**δ ^{31}P (ppm)**	**Compounds P(V)**	**δ ^{31}P (ppm)**	**Δδ (ppm)**	$^1J(^{31}P,^{77}Se)$ (Hz)
[3]$^-$	79.1 (15%) 71.1 (85%)	**[4]$^-$**	35.9 (7%) 33.7 (90%)	-43.2 -37.4	-
		[5]$^-$	73.3 (3%) 71.7 (95%)	-5.8 +0.6	-
		[6]$^-$	73.2 (9%) 69.8 (83%)	-5.9 -1.3	833
[7]$^-$	77.3 (30 %) 73.2 (70 %)	**[8]$^-$**	36.2 (33%) 33.5 (67%)	-41.1 -39.7	-
		[9]$^-$	72.9 (30%) 68.3 (70%)	-4.4 -4.9	-
		[10]$^-$	71.0 (30%) 62.7 (70%)	-6.3 -10.5	848
[11]$^-$	88.3 (90%) 81.9 (10%)	**[12]$^-$**	52.7 (100%)	-35.6	-
		[13]$^-$	95.3 (90%) 92.5 (10%)	+10.6 +10.6	-
		[14]$^-$	98.9 (90%) 94.4 (10%)	+11.3	679
[15]$^-$	96.7 (22%) 89.9 (78%)	**[16]$^-$**	55.2 (50%) 52.2 (50%)	-41.5 -37.7	-
		[17]$^-$	99.9 (20%) 95.2 (80%)	+3.2 +5.3	-
		[18]$^-$	105.0 (10%) 97.5 (90%)	+8.3 +7.5	692

Table 2. Summary of crystallographic data for $[NMe_4]^+$ salts of $[\mathbf{4}]^-$, $[\mathbf{5}]^-$, $[\mathbf{6}]^-$ and $[\mathbf{7}]^-$.

Compound	$[NMe_4][\mathbf{4}]$	$[NMe_4][\mathbf{5}]$	$[NMe_4][\mathbf{6}]$	$[NMe_4][\mathbf{7}]\cdot 0.8CH_2Cl_2$
Formula	$C_{14}H_{37}B_{18}CoNOP$	$C_{14}H_{37}B_{18}CoNPS$	$C_{14}H_{37}B_{18}CoNPSe$	$C_{20.8}H_{40.6}B_{18}CoNP$
M_r	519.93	535.99	582.89	645.94
T/K	293	173	173	173
Crystal system	monoclinic	orthorhombic	orthorhombic	monoclinic
Spacegroup (no.)	*C2/c* (15)	$P2_12_12_1$ (19)	$P2_1nb$ (33)	$P2_1$/c (14)
a (Å)	21.886(5)	10.6695(4)	10.4360(3)	10.508(3)
b (Å)	13.965(5)	14.5788(6)	11.2927(3)	15.676(3)
c (Å)	18.903(3)	17.5974(6)	23.4638(7)	20.258(7)
α (°)	90	90	90	90
β (°)	103.02(2)	90	90	90.323(2)
γ (°)	90	90	90	90
V (Å^3)	5629(3)	2737.25(18)	2765.22(14)	3336.9(16)
Z	8	4	4	4
D_{calc} (g cm^{-3})	1.227	1.301	1.000	1.286
μ(MoK$_\alpha$) (mm^{-1})	0.678	0.0771	2.004	0.708
R_{int}	0.019	0.082	0.065	0.056
Used reflections	4961	5208	5968	5840
Parameters	329	330	329	422
R_1[a]	0.1151 (0.0505)[b]	0.1035 (0.0542)	0.0993 (0.0530)	0.1471 (0.0635)
wR_2[c]	0.1394 (0.1228)	0.1111 (0.0747)	0.1043 (0.0713)	0.1508 (0.0776)
Flack's parameter		0.47(2)		
Largest peak and hole (eÅ^{-3})	0.470 – -320	0.534 – -0.339	0.502 – -0.497	0.776 – -0.534

[a] $R_1 = \Sigma \, | |F_o| - |F_c| \, | \, / \, \Sigma \, |F_o|$

[b] Values in parentheses for reflections with $I > 2.0\sigma(I)$

[c] $wR2 = \{\Sigma \, [\, w(F_o^2 - F_c^2)^2 \,] \, / \, \Sigma \, [w(F_o^2)^2 \,]\}^{1/2}$ and $w = 1/[\sigma^2(F_o^2) + (aP)^2 + bP)]$, where $P = (2F_c^2 + F_o^2)/3$

Table 3. Selected bond lengths (Å) and angles (°) for the anions [**4**]$^-$ – [**7**]$^-$**.**

Compound	**[4]**$^-$	**[5]**$^-$	**[6]**$^-$	**[7]**$^{-\,a}$
	Å	Å	Å	Å
Co(3)-C(1)	2.013(4)	2.017(4)	2.017(5)	2.011(4)
Co(3)-C(1')	2.019(4)	2.013(4)	2.008(6)	1.995(4)
Co(3)-C(2)	2.043(4)	2.037(4)	2.049(5)	2.019(4)
Co(3)-C(2')	2.047(4)	2.052(4)	2.031(6)	2.018(4)
Co(3)-B(8)	2.141(5)	2.135(5)	2.131(7)	2.081(5)
Co(3)-B(8')	2.143(5)	2.134(5)	2.127(6)	2.093(4)
Co(3)-P(1)	2.7668(13)	2.7785(12)	2.7782(15)	2.7687(13)
P(1)-E(1)	1.476(3)	1.9373(16)	2.0904(14)	__
P(1)-C(1)	1.835(4)	1.837(4)	1.819(6)	1.863(4)
P(1)-C(1')	1.844(4)	1.856(4)	1.856(5)	1.915(4)
P(1)-C(13)	1.793(4)	1.802(4)	1.805(5)	1.832(5)
C(1)···C(1')	2.674(6)	2.673(6)	2.658(7)	2.731(6)
C(2)···C(2')	3.887(6)	3.873(7)	3.879(7)	2.896(6)
	°	°	°	°
C(1)-Co(3)-C(1')	83.10(16)	83.13(17)	82.7(2)	85.95(16)
C(1)-P(1)-C(1')	93.24(18)	92.75(18)	92.7(2)	92.55(17)
Co(3)-P(1)-E(1)	120.28(14)	123.75(6)	125.26(6)	__
Co(3)-C(1)-P(1)	91.84(17)	92.13(18)	92.7(2)	91.16(17)
Co(3)-C(1')-P(1)-	91.36(18)	91.72(19)	91.9(2)	90.15(18)
C2-C1···C1'-C2'	-116.3	-118.0	-115.7	1.3

[a] the values in the main component

Table 4. Selected Structural Data for the $[NMe_4]^+$ salts of the studied compounds in comparison with phospha[1]ferrocenophanes ([**19**] and [**20**]). Also data for ions [**21**]$^-$, [**2**]$^-$ and [**22**]$^-$ are included.

Compound	α (deg)[a]	β (deg)[b]	δ (deg)	θ (deg)	M···E (Å)
[**1**]$^-$[47]	+2.0	-	177.6	-	-
[4]$^-$	-9.3(3)	41.4 43.3	174.4	93.2(2)	2.767(1)
[**5**]$^-$	-9.3(2)	41.5 42.6	174.8	92.8(2)	2.779(1)
[**6**]$^-$	-9.5(3)	40.9 41.9	174.6	92.7(2)	2.778(2)
19[25a]	-26.7	32.5	159.8	90.6(3)	2.774(3)
19[25b]	-26.9	32.3	159.8	90.7(2)	2.774(1)
20[26]	-25.4(1)	34.4	161.4	94.3(1)	2.7116(7)
[**21**]$^-$ [11b]	-6.8	43.2	175.6	90.4(1)	2.787(1)
[**2**]$^-$[13b]	+6.8	42.1	174.5	90.3	-
[22]$^-$ [27]	+7.1	42.5	174.2	90.2	-
[c][**7**]$^-$	-3.8(3)	44.0 44.4	177.4	92.6(2)	2.769(1)

[a]The negative value means that the distances between carbon atoms between upper and lower belt have been decreased from the parallel situation (positive value indicates the opposite), [b]two different values refer to β and β', [c]values in the main component.

Table 5. Selected Angles and Distances for the calculated compounds in comparison with calculated phospha[1]ferrocenophanes ([**19**] and [**20**]). The tilt angle α is positive or negative depending on the opening or closure of the C_2B_3 planes around the Co(III) ion.

Compound	α (deg)	β (deg)	δ (deg)	θ (deg)	M···E (Å)
[**19**]	- 27.23	31.46	160.32	89.45	2.812
[**20**]	- 26.03	33.72	161.58	93.28	2.732
[**1**]$^-$	0.00	-	-	-	-
[**2**]$^-$	+ 6.03	-	-	-	-
[**3**]$^-$	- 10.88	40.44	173.87	89.58	2.852
[**4**]$^-$	- 10.71	41.32	173.83	91.84	2.809
[**5**]$^-$	- 10.35	41.02	174.11	90.97	2.831
[**6**]$^-$	- 10.55	41.05	174.35	90.84	2.826
[**7**]$^-$	- 5.75	42.00	175.80	90.82	2.811
[**8**]$^-$	- 5.76	42.59	175.41	92.66	2.774

Table 6. Calculated and experimental ^{31}P NMR chemical shifts for several monoansa and diansa derivatives. Two bridge compounds (μ-P-biphenyl and μ-P(O)-biphenyl) without a metal are included as a comparison.

	Calculated δ(^{31}P)	**Experimental δ(^{31}P)**
[**3**]$^-$	74.9	71.1
[**4**]$^-$	19.6	33.7
[**5**]$^-$	77.6	71.7
[**6**]$^-$	96.3	69.8
[**7**]$^-$	78.0	73.2
[**8**]$^-$	16.9	33.5
μ-P-biphenyl	-6.8	
μ-P(O)-biphenyl	7.8	

Table 7. Calculated diamagnetic and paramagnetic contributions to the ^{31}P NMR for several monoansa and diansa derivatives. Two bridge compounds (μ-P-biphenyl and μ-P(O)-biphenyl) without a metal are included as a comparison.

	Calc. σ_d $\delta(^{31}P)$	**Calc. σ_p $\delta(^{31}P)$**
[**3**]$^-$	-701.7	1066.1
[**4**]$^-$	-702.3	1011.3
[**7**]$^-$	-694.8	1062.3
[**8**]$^-$	-696.7	1003.1
μ-P-biphenyl	-684.7	967.4
μ-P(O)-biphenyl	-679.5	976.8

Table 8. UV/Vis spectra for compounds [**1**]$^-$, [**2**]$^-$, [**3**]$^-$, [**4**]$^-$, [**5**]$^-$, [**7**]$^-$, [**8**]$^-$, [**11**]$^-$, [**15**]$^-$ and [**16**]$^-$ in acetronitrile. λ positions [nm] and ε values [L·cm^{-1}·mol^{-1}] are reported and were calculated following line-fitting analysis.

Compound	λ (ε)								
[**1**]$^-$[38]	220 (15.069)				281 (15.353)		329 (2.171)		445 (496)
[**2**]$^-$	216 (21.571)	236 (13.429)	263 (5.857)	275 (6.286)	285 (12.540)	297 (14.143)	334 (3.403)		517 (586)
[**3**]$^-$	221 (11.099)				284 (15.604)	327 (7.580)	354 (2.067)		461 (616)
[**4**]$^-$	217 (12.702)				278 (7.337)	308 (11.958)	348 (1.835)		460 (252)
[**5**]$^-$	222 (10.789)				283 (5.513)	308 (10.545)	349 (2.088)		456 (461)
[**7**]$^-$	219 (11.223)	240 (8.399)	262 (4.061)	274 (4.271)	289 (6.623)		328 (2.736)	375 (950)	480 (415)
[**8**]$^-$	220 (11.682)	245 (3.689)	263 (3.976)		284 (8.722)	307 (15.693)	342 (2.354)		460 (220)
[**11**]$^-$	210 (7.467)				287 (14.978)	312 (4.197)	340 (2.020)		459 (299)
[**15**]$^-$	230 (10.853)		265 (3.899)	275 (3.248)	287 (9.670)		324 (3.812)	374 (973)	479 (583)
[**16**]$^-$	231 (10.910)		266 (4.176)	274 (4.078)	288 (11.138)		323 (3.730)	365 (1.339)	459 (457)

Table 9. Calculated NPA charges on cobalt, cluster total charge (CTC), energy values (in eV) of the HOMO and LUMO orbitals, their energy difference and experimental $E_{1/2}$ [V/ *fc*] for several monoansa and diansa metallacyclophanes.

Compound	NPA_{Co}	CTC	E_{HOMO}	E_{LUMO}	$\Delta(E_{LUMO}-E_{HOMO})$	$E_{1/2}$ [V]
[**1**]$^-$	-0.460	-3.031	-4.04	0.51	4.54	-1.80
[**2**]$^-$	-0.478	-2.384	-3.23	0.33	3.56	-2.11
[**3**]$^-$	0.314	-3.156	-3.93	0.37	4.30	-1.64
[**4**]$^-$	0.310	-3.219	-4.30	0.19	4.49	-1.43
[**5**]$^-$	0.307	-3.212	-	-	-	-1.47
[**6**]$^-$	0.306	-3.215	-	-	-	-
[**7**]$^-$	-0.646	-2.655	-3.32	0.30	3.63	-1.58
[**8**]$^-$	-0.660	-2.714	-3.46	0.14	3.60	-1.44
[**11**]$^-$	0.312	-3.200	-3.83	0.42	4.26	-1.66
[**15**]$^-$	-	-	-	-	-	-1.85
[**16**]$^-$	-	-	-	-	-	-1.71

References

(1) (*a*) Hawthorne, M. F.; Young, D. C.; Wegner, P. A. *J. Am. Chem. Soc.* **1965**, *87*, 1818. (*b*) Hawthorne, M. F.; Andrews, T. D. *Chem. Commun*. **1965**, 443.

(2) (a) Hawthorne, M.F.; Young, D.C.; Andrews, T.D.; Hove, D.V.; Pilling, R.L.; Pitts, A.D.; Reinjes, M.; Warren, L.F.; Wegner, P.A. *J. Am. Chem. Soc.* **1968**, *90*, 879. (b) Mingos, D. M. P. *J. Chem. Soc, Dalton Trans.* **1977**, 602.

(3) Grabulosa, A. *P-Stereogenic Ligands in Enantioselective Catalysis.* RSC Catalysis Series. Royal Society of Chemistry, 2011.

(4) Rinehart, Jr., A. K.; Frerichs, P. A.; Kittle, L. F.; Westmann, L. F.; Gustafson, R. L.; Pruett, J. E.; McMahon, J. E. *J. Am. Chem. Soc.* **1960**, *82*, 4111.

(5) Osborne, A. G.; Whiteley, R. H. *J. Organomet. Chem.* **1975**, *101*, C27.

(6) For a recent review see: Herbert, D. E.; Mayer, U. F. J.; Manners, I. *Angew. Chem., Int. Ed.* **2007**, *46*, 5060.

(7) Brandt, P. F.; Compton, D. L.; Rauchfuss, T. B. *Organometallics* **1998**, *17*, 2702.

(8) Rojo, I.; Teixidor, F.; Viñas, C.; Kivekäs R.; Sillanpää, R. *Chem. Eur. J.* **2003**, *9*, 4311.

(9) Connelly, N. G.; Geiger, W. E. *Chem. Rev.* **1996**, *96*, 877.

(10) Sivaev, I. B.; Bregadze, V. I. *Collect. Czech. Chem. Commun.* **1999**, *64*, 783.

(11) (a) Chamberlin, R. M.; Scott, B. L.; Melo, M. M.; Abney, K. D. *Inorg. Chem.* **1997**, *36*, 809. (b) Juárez-Pérez, E. J.; Viñas, C.; González-Campo, A.; Teixidor, F.; Sillanpää, R.; Kivekäs, R.; Núñez, R. *Chem. Eur. J.* **2008**, *14*, 4924.

(12) (a) Viñas, C.; Pedrajas, J.; Bertran, J.; Teixidor, F.; Kivekäs, R.; Sillanpää, R. *Inorg. Chem.* **1997**, *36*, 2482. (b) Viñas, C.; Gomez, S.; Bertran, J.; Teixidor, F.; Dozol, J. F.; Rouquette, H. *Chem. Commun.* **1998**, 191. (c) Viñas, C.; Gomez, S.; Bertran, J.; Teixidor, F.; Dozol, J. F.; Rouquette, H. *Inorg. Chem.* **1998**, *37*, 3640. (d) Viñas, C.;

Bertran, J.; Gomez, S; Teixidor, F.; Dozol, J. F.; Rouquette, H.; Kivekäs, R.; Sillanpää, R. *J. Chem. Soc., Dalton Trans.* **1998**, 2849. (e) Viñas, C.; Pedrajas, J.; Teixidor, F.; Kivekäs R.; Sillanpää, R.; Welch, A. J. *Inorg. Chem.* **1997,** *36*, 2988.

(13) (a) Francis, J. N.; Hawthorne, M. F. *Inorg. Chem.* **1971**, *10*, 594. (b) Shelly, K.; Knobler, C. B.; Hawthorne, M. F. *New J. Chem.* **1988**, 317.

(14) (a) Mortimer, M. D.; Knobler, C. B.; Hawthorne, M. F. *Inorg. Chem.* **1996**, *35*, 5750. (b) Rojo, I.; Teixidor, F.; Kivekäs, R.; Sillanpää, R.; Viñas, C. *Organometallics* **2003**, *22*, 4642. (c) Beletskaya, I. P.; Bregadze, V. I.; Ivushkin, V. A.; Petrovskii, P. V.; Sivaev, I. B.; Sjöberg, S.; Zhigareva, G. G. *J. Organomet. Chem.* **2004**, *689*, 2920.

(15) Farràs, P; Olid-Britos, D.; Viñas, F.; Teixidor, F. *Eur. J. Inorg. Chem.* **2011**, 2525.

(16) (a) Plesek, J.; Hermánek, S.; Base, K.; Todd, L. J.; Wright, W. F. *Collect. Czech. Chem. Commun.* **1976**, *41*, 3509. (b) González-Cardoso, P.; Stoica, A.-I.; Farràs, P.; Pepiol, A.; Viñas, C.; Teixidor, F. *Chem. Eur. J.* **2010**, *16*, 6660.

(17) (a) Teixidor, F.; Viñas, C.; Abad, M. M.; Kivekäs, R.; Sillanpää, R. *J. Organomet. Chem.* **1996**, *509*, 139. (b) Viñas, C.; Núñez, R.; Teixidor, F.; Sillanpää, R.; Kivekäs, R. *Organometallics* **1999**, *18*, 4717.

(18) Verkade, J. G.; Mosbo, J. A. *Phosphorus-31 NMR Spectroscopy in Stereochemical Analysis*; Quin, L. D., Verkade, J. G., Eds.; VCH: New York, 1987.

(19) McFarlane, W.; Rycroft, D. S. *J. Chem. Soc., Dalton Trans*. **1973**, *20*, 2162.

(20) Allen, D. W.; Taylor, B. F. *J. Chem. Soc., Dalton Trans*. **1982**, 1, 51.

(21) Jameson, C. J. *Phosphorus-31 NMR Spectroscopy in Stereochemical Analysis*; Quin, L. D., Verkade, J. G., Eds.; VCH: New York, 1987.

(22) Klapötke, T. M.; Broschag, M. *Compilation of Reported 77Se NMR Chemical Shifts*, Wiley, Chichester, **1996**.

(23) Burford, N.; Royan, B. W.; Spence, R. E. v. H.; Rogers, R. D. *Dalton. Trans.* **1990**, *7*, 2111.

(24) Pyykkö, P.; Atsumi, M. *Chem. Eur. J.* **2009**, *15*, 12770.

(25) (a) Stoeckli-Evans, H.; Osborne, A. G.; Whiteley, R. H. *J. Organomet. Chem*. **1980**, *194*, 91. (b) Butler, I. R.; Cullenm, W. R.; Einstein, F.W. B.; Rettig, S. J.; Willis, A. J. *Organometallics* **1983**, *2*, 128.

(26) Patra, S. K.; Whittell, G. R.; Nagiah, S.; Ho, C.-L.; Wong, W.-Y.; Manners, I. *Chem. Eur. J*. **2010**, *16*, 3240.

(27) Rojo, I.; Kivekäs, R.; Teixidor, F.; Sillanpää, R.; Viñas, C. *J. Am. Chem. Soc*. **2003**, *125*, 14720.

(28) Cook, J. B.; Nicholson, B. K.; Smith, D. W. *J. Organomet. Chem*. **2004**, *689*, 860, and references therein.

(29) Popescu, A. R.; Laromaine, A.; Teixidor, F.; Sillanpää, R.; Kivekäs, R.; Llambias, J. I.; Viñas, C. *Chem. Eur. J*. **2011**, *17*, 4429.

(30) Allen, F. H. *Acta Crystallogr.* **2002**, *B58*, 380.

(31) CSD codes AMCOCB10, AMCOCB, CAKXOC, GOCBEF, IQAKIV, GOPNOO, RULMOA, WUJZUW and WUJZOQ.

(32) Bondi, A. *J. Phys. Chem.* **1964**, *68*, 441.

(33) Bader, R. F. W. *Atoms in Molecules: a Quantum Theory*; Clarendon Press, Oxford: New York, 1990.

(34) Todd, L. J.; Siedle, A. R., *Progress in NMR Spectroscopy* **1979**, *13*, 87.

(35) (a) Grimes, R. N. *Carboranes Second Edition*; Elsevier: New York/Oxford, 2011. (b) Hermanek, S.; Plesek, J.; Stibr, B.; Grigor, V. *J. Chem. Soc., Chem. Commun.* **1977**, 561. (c) Stanko, V. I.; Babushkina, T. A.; Klimova, T. P.; Goltyapin, Y. U.; Klimova,

A. I.; Vasilev, A. M.; Alymov, A. M.; Khrapov, V. V. *Zh. Obshch. Khim.* **1976**, *46*, 1071. (d) Teixidor, F.; Viñas, C.; Rudolph, R. W. *Inorg. Chem.* **1986**, *25*, 3339.

(36) (a) Bühl, M.; Hnyk, D.; Machácek, J. *Chem. Eur. J.* **2005**, *11*, 4109. (b) Pennanen, T. O.; Machácek, J.; Taubert, S.; Vaara, J.; Hynk, D. *Phys. Chem. Chem. Phys*. **2010**, *12*, 7018.

(37) Parish, R. V. *NMR, NQR, EPR, and Mössbauer spectroscopy in Inorganic Chemistry*, Ellis Horwood Series in Inorganic Chemistry. Series Editor J. Burgess. Ellis Horwood Limited, West Sussex, England, 1990.

(38) Rojo, I.; Teixidor, F.; Viñas, C.; Kivekäs, R.; Sillanpää, R. *Chem. Eur. J.* **2004**, *10*, 5376.

(39) (a) Teixidor, F.; Núñez, R.; Viñas, C.; Sillanpää, R.; Kivekäs, R. *Angew. Chem., Int. Ed.* **2000**, *39*, 4290. (b) Núñez, R.; Farràs, P.; Teixidor, F.; Viñas, C.; Sillanpää, R.; Kivekäs, R. *Angew. Chem., Int. Ed.* **2006**, *45*, 1270. (c) Teixidor, F.; Núñez, R.; Viñas, C.; Kivekäs , R. ; Sillanpää, R. *Inorg. Chem.* **2001**, *40*, 2587.

(40) Manners, I. "Ring-Opening Polymerization of Metallocenophanes: A New Route to Transition Metal-Based Polymers", *Advances in Organometallic Chemistry*, Vol. 37, Academic Press, New York, 1995.

(41) Pudelski, J. K.; Foucher, D. A.; Honeyman, C. H.; Lough, A. J.; Manners, I.; Barlow, S.; O'Hare, D. *Organometallics* **1995**, *14*, 2470.

(42) Oliva, J. M.; Viñas, C. *J. Mol. Struct.* **2000**, *556*, 33.

(43) (a) Lever, A. B. P. *Inorg. Chem.* **1990**, *29*, 1271. (b) Lever, A. B. P. *Inorg. Chem.* **1991**, *30*, 1980. (c) Lever, A.B.P.; Dodsworth, E.S. *Inorganic Electronic Structure and Spectroscopy*; Solomon, E.I, Lever, A.B.P, Eds.; Wiley: New York, 1999; vol. 2, pp. 227–287.

(44) Matel, L.; Macásek, F.; Rajec, P.; Hermánek, S.; Plesek, J. *Polyhedron* **1982**, *1*, 511

(45) Cerný, V.; Pavlík, I.; Kustková-Maxová, E. *Collect. Czech. Chem. Communn.* **1976**, *41*, 3232.

(46) Fally, S.; Carleer, M.; Vandaele, A. C. *J. Quant. Spectrosc. Ra.* **2009**, *110*, 766.

(47) Juárez-Pérez, E. J.; Núñez, R.; Viñas, C.; Sillanpää, R.; Teixidor, F. *Eur. J. Inorg. Chem*. **2010**, 2385.